

**VERY LARGE FLOATING CONTAINER TERMINAL  
AND OPTIMAL LAYOUT OF GILL CELLS**

**YAO ZIJIAN**

**NATIONAL UNIVERSITY OF SINGAPORE**

**2007**

**VERY LARGE FLOATING CONTAINER TERMINAL  
AND OPTIMAL LAYOUT OF GILL CELLS**

**YAO ZIJIAN**

**(B.Eng., Shanghai Jiao Tong University)**

**A THESIS SUBMITTED  
FOR THE DEGREE OF MASTER OF ENGINEERING  
DEPARTMENT OF CIVIL ENGINEERING  
NATIONAL UNIVERSITY OF SINGAPORE**

**2007**

## **ACKNOWLEDGEMENTS**

Firstly, I would like to thank Jurong Consultants Pte Ltd. for providing me with a research scholarship and a great opportunity to pursue my graduate study at National University of Singapore.

Secondly, I would like to thank my supervisor, Professor Wang Chien Ming, for his useful advice and continuous guidance throughout my study at the Department of Civil Engineering, National University of Singapore.

Thirdly, I am grateful to all my fellow graduate students in the Center for Offshore Research and Engineering for the many useful discussions.

Last but not least, I owe my heartfelt thanks to my parents and all my friends, for their help and kind encouragement.

## TABLE OF CONTENTS

ACKNOWLEDGEMENTS .....	i
TABLE OF CONTENTS .....	ii
SUMMARY .....	iv
LIST OF NOTATIONS .....	vii
LIST OF FIGURES .....	ix
LIST OF TABLES .....	xi
CHAPTER 1 - INTRODUCTION TO FLOATING STRUCTURES.....	1
1.1 Sea Space Utilization .....	1
1.2 Introduction to Very Large Floating Structures (VLFS).....	4
1.3 Objective and Scope of Study.....	7
1.4 Layout of Thesis.....	8
CHAPTER 2 - SUPER-LARGE FLOATING CONTAINER TERMINALS.....	10
2.1 Floating Container Terminals.....	10
2.2 Preliminary Design .....	13
CHAPTER 3 - MODELING, STATIC ANALYSIS AND DETAIL DESIGN OF CONTAINER TERMINAL.....	22
3.1 Modeling of Floating Container Terminal .....	22
3.2 Static Analysis of Floating Container Terminal .....	24
3.3 Detail Design of a Typical Watertight Cell .....	28
CHAPTER 4 - CONTROLLING DESIGN CRITERION AND GILL CELL CONCEPT.....	46
4.1 Introduction.....	46
4.2 The Concept of Gill Cells .....	46
4.3 Effect of Gill Cells .....	50
CHAPTER 5 - OPTIMAL LAYOUTS OF GILL CELLS.....	53

5.1 Proposed Location Patterns of Gill Cells.....	53
5.2 Optimization of the Gill Cells' Locations using Genetic Algorithms.....	59
5.3 Layouts of Gill Cells for Different Loading Patterns and Shapes of VLFS ....	75
 CHAPTER 6 - CONCLUSIONS AND RECOMMENDATIONS FOR FUTURE STUDIES .....	 76
6.1 Conclusions.....	76
6.2 Recommendations for Future Research.....	78
 REFERENCES .....	 79
 APPENDIX A - GENETIC ALGORITHMS .....	 81
Roulette Wheel Selection.....	81
Reproduction (Crossover and Mutation) .....	82
 APPENDIX B - COMPUTER CODE .....	 84
Genetic Function.....	84
Objective Function.....	85
Execution of the First Generation.....	86

## SUMMARY

In recent years, city planners and engineers of land-scarce countries or countries with long coastlines have resorted to the use of very large floating structures (VLFS) to create land from the sea. Japan is the world's leader in VLFS, having constructed many floating structures including the largest pontoon-type floating structure (called the Mega-Float) as a test airplane runway in Tokyo Bay. The Mega-Float measures 1000m x 60-120m x 3m.

Nowadays, as the demands for container shipment increases, there is a trend to build larger container ships. But these mega-container ships with 10000 to 15000 TEUs capacity can only call at several ports. In Singapore's port expansion plans, future ports must be able to accommodate the berthing of these mega-container ships. Coupled by the lack of fill materials for land reclamation needed in the construction of the mega ports in deep waters and the need to preserve the coastal environment and current flow, Singapore is exploring the feasibility of constructing a super large floating container terminal.

In this study, we conduct research on a very large floating container terminal for use in Singapore waters. Based on the functional and operational requirements given by PSA and MPA engineers, a preliminary sizing of the floating container terminal with dimensions 520m x 470m x 10m is proposed. The floating container terminal is to be constructed from high performance concrete. Using a finite element model, static analyses were performed for the floating container terminal under immense live load

due to the 7-tier container loading on its central stacking yard. As a consequence of such a central loading, the floating container terminal undergoes a dish-like deformation. The differential deflection between the central portion and the edges and corners of the floating container terminal is relatively large. This poses a problem as the smooth operation of the quay cranes requires a very stringent between-rail gradient tolerance. The differential deflection causes this tolerance to be violated, rendering the quay cranes non-operational. It is clear that the differential deflection is the controlling factor in the design and ways to mitigate this must be found. By increasing the top and bottom slab thicknesses, or the height of the floating structure, or by using a larger draft for the central portion of the structure will increase the flexural stiffness of the structure and thereby decreasing the differential deflection. But these remedies will add much cost to the super-large floating container terminal. An innovative and cost effective solution was found in the form of “gill cells” in order to reduce the differential deflection between the edge areas and the central portion. These gill cells are compartments in the floating structure where the bottom surface is perforated to allow water to flow freely in and out. At the locations of these gill cells, the buoyancy forces are eliminated. When placed appropriately, say at the edges in the case of the floating container terminal, we remove the buoyancy forces at the edge and hence create hogging moments that reduce the central deflection. It will be shown here that the differential deflection is indeed considerably minimized. Moreover, the bending stresses are reduced at the same time as a result of reducing the curvature of the floating structure. For maximum effectiveness of gill cells and economic savings, it is

important that the optimal layout of gill cells be determined. Therefore, Chapter 5 of this thesis is devoted to the optimization study of gill cells. A general technique, based on genetic algorithms and used in conjunction with ABAQUS for the structural analysis, is developed and demonstrated on floating structures with various shapes and subjected to various loading configurations. The optimal solution will be compared with intuitive design of gill cell location to assess the sensitivity of the differential deflection with respect to the gill cells locations.



## LIST OF NOTATIONS

$Q_k$	Characteristic imposed load
$G_k$	Characteristic dead load
$n$	Total design ultimate load per unit area
$\lambda_x$	Length of shorter side
$\lambda_y$	Length of longer side
$\beta_{sx}, \beta_{sy}$	Bending moment coefficients
$m_{sx}$	Maximum design ultimate moments either over supports or at mid-span on strips of unit width and span $\lambda_x$
$m_{sy}$	Maximum design ultimate moments either over supports or at mid-span on strips of unit width and span $\lambda_y$
$b$	Breadth of slab under consideration
$d$	Effective depth of the tension reinforcement
$d'$	Depth to the compression reinforcement
$K$	Parameter used for calculating the lever arm $z$
$z$	Lever arm
$A_s$	Area of tension reinforcement
$A_s'$	Area of compression reinforcement
$\beta_{vx}, \beta_{vy}$	Shear force coefficients
$V$	Shear force due to design ultimate loads or the design ultimate value of a concentrate load

$v$	Nominal design shear stress
$v_c$	Design ultimate shear stress
$\gamma_m$	Partial safety factor for strength of material
$f_{cu}$	Characteristic strength of concrete
$A_{sv}$	Area of shear links in a zone
$s_v$	Spacing of links
$f_{yv}$	Characteristic strength of shear reinforcement
$f_s$	Estimated design service stress in tension reinforcement
$\alpha_{cr}$	Distance from cracking point to nearest bar
$\rho$	Area of tension steel relative to concrete in a section
$A_{st}$	Area of steel in tension
$\rho_1$	Area of compression steel relative to concrete in a section
$A_{sc}$	Area of steel in compression
$\alpha_e$	Modular ratio = $\frac{E_s}{E_c}$
$E_s$	Young's modulus of steel
$E_c$	Young's modulus of concrete
$x$	Depth of neutral axis
$I$	Second moment of area
$w_d$	Crack width

## LIST OF FIGURES

Fig. 1.1 Kansai International Airport .....	3
Fig. 1.2 Kamigoto oil storage base .....	3
Fig. 1.3 Applications of VLFS .....	5
Fig. 1.4 Components of a Pontoon-type VLFS.....	6
Fig. 2.1 Floating terminal complex with 20 modular berths.....	12
Fig. 2.2 Option 1 layout for very large floating container terminal.....	19
Fig. 2.3 Option 2 layout for very large floating container terminal.....	20
Fig. 2.4 Dimensions of a compartment in floating container terminal .....	21
Fig. 3.1 Finite element model for floating container terminal .....	24
Fig. 3.2 Deflection contours for the three load cases.....	26
Fig. 3.3 Loaded area of floating container terminal.....	26
Fig. 3.4 Compartments of the floating container terminal.....	28
Fig. 3.5 Position that crack may occur.....	33
Fig. 3.6 (a) Plan view and (b) side view of the cell with reinforcement details ....	39
Fig. 3.7 Loading condition of the compartment walls .....	40
Fig. 4.1 Cross-sectional portion of the floating structure with gill cells.....	48
Fig. 4.2 Examples of shapes and locations of slits/holes for gill cells.....	48
Fig. 4.3 Proposed location of gill cells when floating structure is loaded in the center portion .....	49
Fig. 4.4 Side view of floating structure.....	49
Fig. 4.5 Plan view of floating structure.....	50

Fig. 4.6 Deflection surfaces of the floating container terminal with and without gill cells.....	51
Fig. 4.7 Stress contours of the floating container terminal with and without gill cells.....	52
Fig. 5.1 Floating structure carrying heavy loads in the central portion .....	55
Fig. 5.2 Loading and boundary condition of a quarter of the structure .....	55
Fig. 5.3 Pattern 1 of gill cells' location .....	56
Fig. 5.4 Pattern 2 of gill cells' location .....	57
Fig. 5.5 Pattern 3 of gill cells' location .....	58
Fig. 5.6 Patterns 4 and 5 of gill cells' location.....	58
Fig. 5.7 Flow chart of the basic steps in genetic algorithm .....	60
Fig. 5.8 Procedure of GA interfacing with ABAQUS .....	60
Fig. 5.9 Convergence of differential deflection with respect to generations .....	67
Fig. 5.10 Layouts of the gill cells through “coarse identification” model.....	68
Fig. 5.11 Quadrant of floating structure showing loaded area and location of gill cells.....	69
Fig. 5.12 Convergence of differential deflection with respect to number of generations .....	71
Fig. 5.13 Layouts of the gill cells through “refinement” model .....	68
Fig. 5.14 Optimal layout of gill cells with 20% gill cells .....	73
Fig. 5.15 Comparison between various patterns of gill cells layouts .....	73
Fig. 5.16 Optimal layout of gill cells with 10% gill cells .....	74
Fig. 5.17 (a) Loading area and (b) Optimal layout of gill cells for floating structure with $L/B=4$ .....	75

## LIST OF TABLES

Table 2.1 General conditions .....	13
Table 2.2 Natural conditions .....	14
Table 2.3 Loading conditions.....	14
Table 2.4 Design data for cargo gear .....	15
Table 2.5 Tolerances for design of traveling rail (for concrete runway).....	16
Table 2.6 Access bridge .....	17
Table 3.1 Critical deflection of floating structure.....	25
Table 3.2 Cranes' gradients.....	26
Table 3.3 Principal stresses at top and bottom slab.....	27
Table 3.4 Deflections and drafts .....	27
Table 4.1 Crane gradient with gill cells .....	51
Table 4.2 Principal stresses at top and bottom slabs with gill cells .....	51
Table 4.3 Deflection and drafts with gill cells .....	51
Table 5.1 Corresponding differential deflection and gradients associated to gill cells layout 1 .....	56
Table 5.2 Corresponding differential deflection and gradients associated to gill cells layout 2 .....	57
Table 5.3 Corresponding differential deflection and gradients associated to gill cells layouts 3, 4, 5.....	58

# **INTRODUCTION TO FLOATING STRUCTURES**

## **1.1 Sea Space Utilization**

Before the 20<sup>th</sup> Century, human activities such as mining, farming and energy production have been basically confined to land, which only takes 29 percent of the earth surface area whereas 71 percent of the earth surface is covered by water. In the last few decades, continuous exploitations, growing populations and developing economies have stretched land resources to their limits. This limitation has forced people to colonize and exploit the ocean for space, energy, water food and even to store carbon dioxide to mitigate global warming.

There are many directions in modern sea space utilization. Besides the traditional harbor engineering, offshore jack-up rigs for oil drilling and the maritime transportation, new sea space utilization focuses on the construction of offshore artificial cities, offshore power stations, marine parks, offshore airports, submarine tunnels and submarine warehouses and so on. People are currently constructing or designing various artificial islands, very large floating structures and submarine engineering structures used for offshore oil and natural gas production, working and living environment. For instance, the most famous Burj al-Arab, a luxurious hotel on a man-made island in Dubai, United Arab Emirates and the Treasure island in San Francisco Bay, USA.

In the exploitation of ocean space, as we all know, Netherlands, Japan, Norway and USA are the pioneers in the utilization of sea space. The sea reclamation of Netherlands was once regarded as a miracle. Netherlands has an area of 41,528 square kilometers and a population of about 16 million. As it is a lowland country (approximately half of the country's land is below or at the sea level), the Dutchmen have been fighting against sea throughout all these years. As early as the 13<sup>th</sup> century, Dutchmen constructed the dykes to hold back sea water. Through hundreds of years, the Dutchmen constructed as long as 1800 kilometers dykes and at the mean time, increased their land area by six thousand square kilometers. Now, 20 percent of the land area of Netherlands is created from land reclamation. Japan is an island country with a total land area of 0.38 million square kilometer. Of the land areas, 80% is mountainous and most human activities are concentrated on the plains along the shoreline. Ocean space utilization has been a key priority for Japan. Until the 20<sup>th</sup> century, reclamation of shallow waters has been the only technology available to expand human activities onto the sea. Kansai International Airport (Fig. 1.1) was a wonder built on the reclaimed land. In the late of 1950s, architects in Japan had proposed the concept of ocean space utilization using a floating structure and in the following several decades, more and more research on the very large floating structure technology had been performed. Following this trend, the technology of very large floating structure has been being developed at a high speed. The construction of the Kamigoto and Shirashima oil storage base (Fig. 1.2) and other floating structures had shown the advanced state of the Japanese in the large floating structures technology.

The same as Netherlands and Japan, in the last several decades, Norway and USA developed very fast in the ocean space utilization, especially on the designing and constructing floating structures for various kind of purpose.



*Fig. 1.1 Kansai International Airport*  
([www.mlit.go.jp/.../02\\_international/kansai.html](http://www.mlit.go.jp/.../02_international/kansai.html))



*Fig. 1.2 Kamigoto oil storage base*  
(Suzuki, 2005)



The 21<sup>st</sup> century will likely be the century that people explore the ocean space limits and colonize the ocean for habitation and development.

## 1.2 Introduction to Very Large Floating Structures (VLFS)

A very large floating structure (VLFS) is a relatively new technology for creating land from the sea. As population and urban development expand in the land-scare island countries (or countries with long coastlines), city planners and engineers of these countries have resorted to land reclamation from the sea in order to reduce the pressure on existing land shortage problem. However, there are some disadvantages in land reclamation, such as the negative environmental effect on the country's and neighboring country's coastlines and marine eco-system, soil settlement problems and the huge economic costs in reclaiming land from deep coastal waters. Because of the requirement of land usage and the problems in land reclamation work, engineers have proposed the construction of very large floating structures (VLFS) for industrial space, airports, and storage facilities. Figure 1.3 shows some applications of VLFS such as floating airport, floating emergency rescue base, floating container terminal, floating sports facilities, floating leisure industry and floating waste process facility.



**floating airport**



**floating emergency  
rescue base**



**floating container terminal**



**floating sports facility**



**floating leisure industry**



**floating waste  
process facility**

*Fig. 1.3 Applications of VLFS*

VLFS may be classified to two categories, i.e. the pontoon-type and the semi-submersible-type. The pontoon-type of floating structure is a simple flat box structure, like a giant plate floating on the water. It features high stability, low manufacturing cost and easy maintenance and repair. However, the pontoon-type structures can only be constructed in calm waters associated with naturally sheltered coastal formations. In contrast, the semi-submersible-type of floating structure is raised above the sea level using column tubes or ballast structural elements. It is suitable for open seas where there are large waves since it is able to minimize the effects of waves while maintaining a constant buoyant force. The super-large floating container terminal that we are concern about in this thesis is to be constructed in calm waters, and it is a pontoon-type floating structure.

Referring to Fig. 1.4, a pontoon-type floating structure system consists of the following components:

- A very large pontoon-type floating structure
- Station keeping system to keep the floating structure in place
- An access bridge or a floating road to get to the floating structure from shore
- A breakwater for reducing wave forces impacting the floating structure

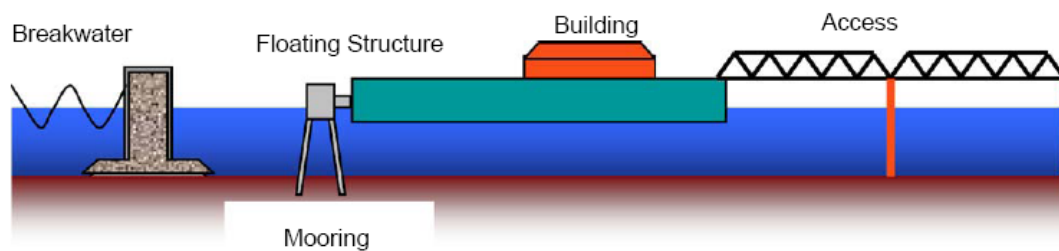


*Fig. 1.4 Components of a Pontoon-type VLFS*

Very large floating structures have many advantages over the traditional land reclamation solution for birthing land from the sea. Their advantages include:

- They are cost effective when the water depth is large and the seabed is soft
- Environmental friendly as they do not damage the marine eco-system, or silt-up deep harbors or disrupt the tidal/ocean currents
- They are easy and fast to construct (components may be made at different shipyards and then brought to the site for assembling)
- They can be easily removed (if the sea space is needed in future) or expanded (since they are of a modular form)
- The facilities and structures on very large floating structures are protected from seismic shocks since they are inherently base isolated.
- They do not suffer from differential settlement due to reclaimed soil

consolidation

- Their positions with respect to the water surface are constant and thus facilitate small boats and ship to come alongside when used as piers and berths
- Their location in coastal waters provide scenic body of water all around, making them suitable for developments associated with leisure and water sport activities
- Their interior spaces may be used for car parks, offices, etc.
- There is no problem with rising sea level due to global warming

### 1.3 Objective and Scope of Study

In this study, we conduct research on a very large floating container terminal for use in Singapore waters. The objectives of this study are:

- To present a preliminary design of the floating container terminal based on the functional and operational requirements given by PSA and MPA engineers.
- To model and perform static analyses of the floating container terminal under self-weight and live load (due to container loadings) on the central stacking yard. The finite element software ABAQUS is used for the analyses.
- To solve the problem of large differential deflection in the floating container terminal that violates the serviceability requirement for the quay crane rails. The proposed solution takes the form of the innovative gill cells concept in order to reduce the differential deflection between central portion and corners of the floating container terminal so as to ensure the smooth operation of the

quay cranes.

- To develop a numerical technique and computer code for determining the optimal layouts of gill cells on floating structures of various shapes and under different loading patterns. The technique makes use of genetic algorithms as well as it involves the development of an interfacing code to link the genetic algorithms to the finite element software ABAQUS. Optimal layouts of gill cells are determined for example problems and the effectiveness of the optimal solution is measured by considering other layouts.

## 1.4 Layout of Thesis

There are 6 chapters in this thesis. Chapter 1 provides a general introduction to the utilization of sea space and very large floating structures as well as presents the objectives of this research study. In Chapter 2, we introduce the preliminary design of a very large floating container terminal made from high performance concrete. Based on the functional and operational requirements given by PSA and MPA engineers, a preliminary sizing of the floating container terminal with dimensions 520m x 470m x 10m is proposed. Chapter 3 focuses on the modeling and static analysis of the floating container terminal and the detail design of a typical watertight compartment of the floating container terminal. Using a finite element model, static analyses were performed for the floating container terminal under self-weight and the immense live load due to the multiple tiers of container piled up on its central stacking yard. As a consequence of such a central loading, the floating container terminal undergoes a

dish-like deformation. The differential deflection between the central portion and the edges and corners of the floating container terminal is relatively large. This poses a problem as a very stringent between-rail gradient tolerance is required for the smooth operation of the quay cranes. The differential deflection causes this tolerance to be violated, rendering the quay cranes non-operational. It is clear that the differential deflection is the controlling factor in design and ways to mitigate this must be found.

In Chapter 4, an innovative and cost effective solution is proposed in the form of “gill cells” in order to reduce the differential deflection between the edge areas and the central portion of the floating container terminal. These gill cells are compartments in the floating structure where the bottom surface is perforated to allow water to flow freely in and out. At the locations of these gill cells, the buoyancy forces are eliminated. When placed appropriately, say at the edges in the case of the floating container terminal, the removal of the buoyancy forces at the edge creates hogging moments at the edges that assist in reducing the central deflection. The effectiveness of gill cells in minimizing the differential deflection and bending stresses are also demonstrated in Chapter 4. For maximum effectiveness of gill cells and economic savings, it is important that the optimal layout of gill cells is determined. Thus, Chapter 5 is devoted to the optimal layout of gill cells. A general technique, based on genetic algorithms and used in conjunction with ABAQUS structural analysis software, is developed and demonstrated on floating structures with various shapes and subjected to various loading configurations. Finally, Chapter 6 presents the conclusions of the study and recommendations for future research.

## **SUPER-LARGE FLOATING CONTAINER TERMINALS**

### 2.1 Floating Container Terminals

There is a trend to build larger container ships as the demand for container shipment increases. In the present time, these mega-container ships with 10,000 to 15,000 TEUs capacity can only call at several ports in United States and Europe (Baird, 2002). This is because most existing ports do not have the dimensions, layout and quay cranes to accommodate these ships with length of about 400m and the required water depth of at least 20m. Therefore, in the expansion plans of Singapore's container terminals, the design of terminals must be able to cater for such mega-vessels.

All the ports in Singapore are built on reclaimed land due to the acute shortage of firm land. The land reclamation solution is cost effective provided that the water depth is shallow and fill materials are available at a reasonably cheap price. However, when faced with large water depths and very costly fill materials, the land reclamation option becomes an expensive solution. The alternative solution is to construct a very large floating structure (VLFS) to provide the artificial piece of land in deep waters for the mega ship container terminal.

These very large floating container terminals have advantages over their traditional land reclamation counterparts in the following respects:

- They are cost effective when the water depth is large and the seabed is soft

- Environmental friendly as they do not damage the marine ecosystem, or silt-up deep harbors or disrupt the tidal/ocean currents
- They are easy and fast to construct (components may be made at different shipyards and then brought to the site for assembling) and therefore sea-space can be speedily exploited
- They can be easily removed (if the sea space is needed in future) or expanded (since they are of a modular form)
- Their positions with respect to the water surface are constant and thus facilitate ship to come alongside

In response to the need for large container terminals and the advantages of floating structures over land reclamation option, a systematic research study on the feasibility and cost effective design of very large floating container terminal is of prime importance to Singapore (Wang and Wu, 2005).

PSA proposed the construction of a 4.7km x 1.08km container terminal complex for the future expansion plan of Singapore ports. The water depth for the site ranges from 15m to 20m. The terminal is to be served by a central spine road running longitudinally. The container terminal may be built on either reclaimed land or on 20 VLFS modules or on partly reclaimed land and partly on VLFS. Each module will cover an area of 470m x 520m to accommodate the berthing of mega-ships as long as 400m. The layout of the floating terminal complex with 20 modular berths is shown in Fig. 2.1.



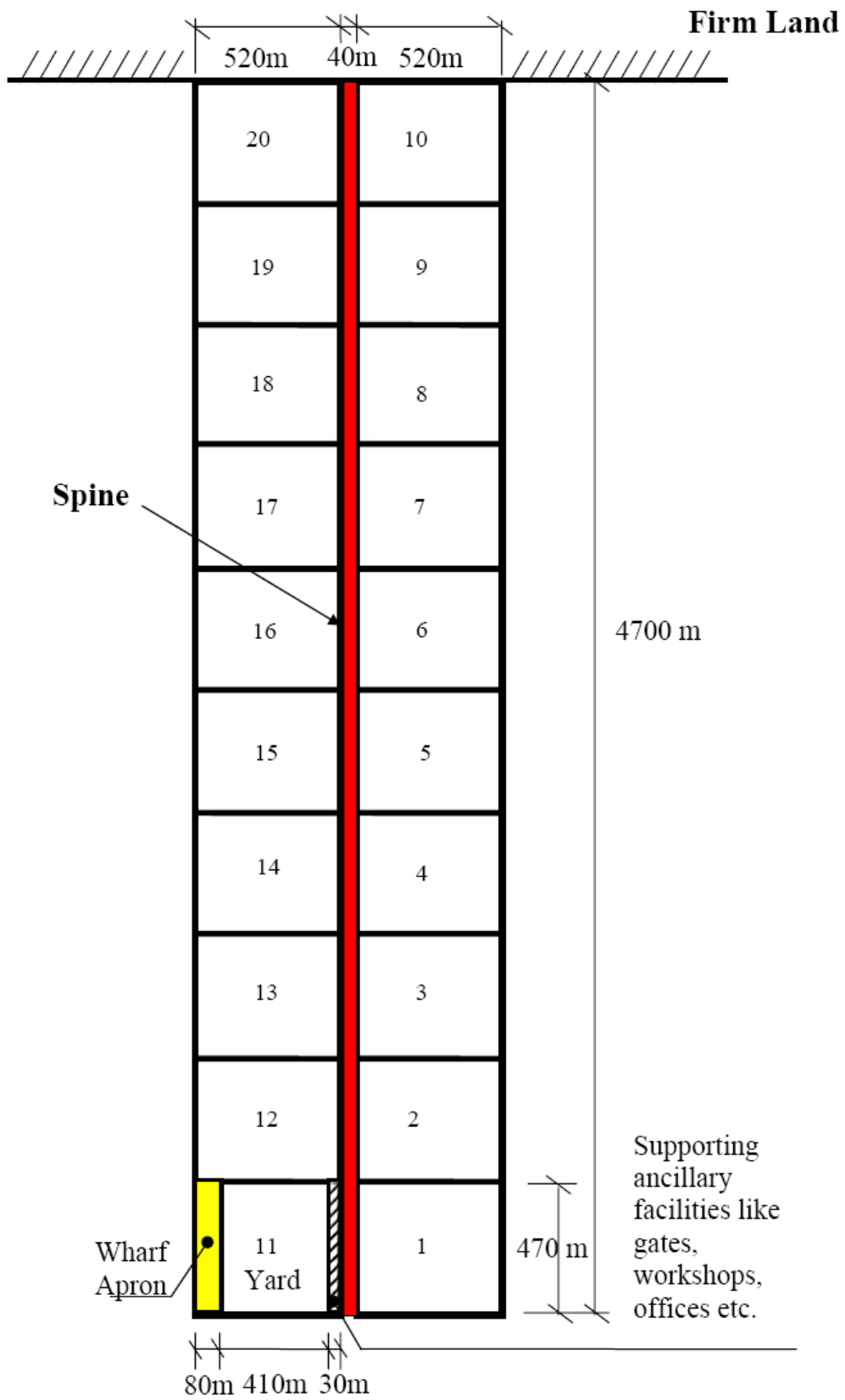


Fig. 2.1 Floating terminal complex with 20 modular berths

## 2.2 Preliminary Design

The floating container terminal complex comprises of 20 modular berths. In this study, we focus on the modeling, analysis and design of a single floating module for the berth and central stacking yard. The following design data and pertinent information given in Tables 2.1 to 2.6 have been furnished by PSA, MPA and JCPL engineers for the feasibility study of this 470m x 520m x 10m super-large floating container terminal.

*Table 2.1 General conditions*

Design Ship of Container Terminal		12,500 TEU Capacity Ship
Berth	Designed Water Depth	16 m
	Number of Berth	10
	Length	470 m
Breadth of Apron		80 m
Life Span		50 years
Type of Mooring Facility		<p>Could be any type as long as it fulfils its intended function and it should not:</p> <ul style="list-style-type: none"> <li>▪ Reduce the wharf length</li> <li>▪ Cause obstruction to berthing/unberthing of ships</li> <li>▪ Cause obstruction to the smooth terminal operation when operating alone or when operating with more than one module</li> <li>▪ Disable the advantage of linear berth when more than one module is put in operation, i.e. there should not be any vertical protrusion in the yard or horizontal protrusion beyond the wharf line by the mooring system</li> </ul>
Floating Structure	Dimensions L × B × D	470 m × 520 m × 10 m
	Freeboard	2.5 m

Table 2.2 Natural conditions

Tide	High Water Level (HWL)		3.0 m
	Low Water Level (LWL)		0.0 m
	Water Depth		16.0 m
Wind	Operation (Vessel Moored) Velocity		15.0 m/sec
	Storm (Without Vessel) Velocity		20.0 m/sec (about 40 knots)
Wave	Operation (Vessel Moored)	Height, $H_{1/3}$	0.5 m
		Period, $T_{1/3}$	5.0 sec
	Storm (Without Vessel)	Height, $H_{1/3}$	1.0 m
		Period, $T_{1/3}$	5.0 sec
Tidal Current Speed			1.8 m/sec (about 3.5 knots)
Soil Condition under Sea Bed			Hard Strata/Rock; SPT>60

Table 2.3 Loading conditions

Size of Vessel			120,000 DWT for a 12,500 TEU capacity ship
Approach Speed			15 cm/sec
Bollard Pull			150 t/set
Load on Floating Structure	Apron	Operation	3 t/m <sup>2</sup>
	Behind Apron	Operation	$9 \times 24 \text{ ton} / (6.55 \times 2.74) = 12 \text{ ton/m}^2$ by assuming 7 high stacking.
Storage of Container (Row $\times$ Tier)			6 $\times$ 9
Maximum Gross Mass	Loaded Containers	20 ft x 8 ft x 8 ft	24 t
		40 ft x 8 ft x 8-9.5 ft	30 t
Thickness of Pavement			10 cm

Table 2.4 Design data for cargo gear

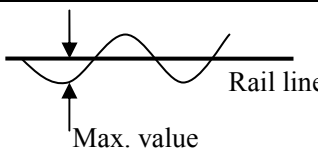
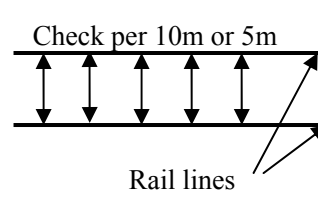
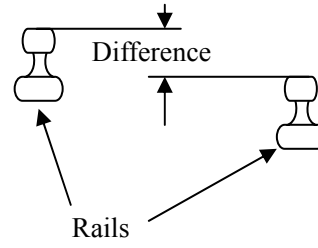
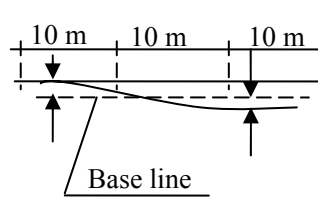
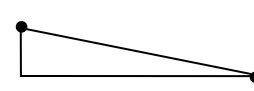
Gantry crane for cargo gear

Number of Crane		8 sets
Rated Load		65 t
Outreach		70 m
Traveling Distance		425 m
Rail Span		30.5 m
Lifting Length	(under)	16.2 m
	(upper)	40 m
Winding Speed	(loaded)	90 m/min
	(no-load)	180 m/min
Traveling Speed		60 m/min
Crane Weight		1,360 t
Wheel Load	Sea Side	980 KN at 1.219 m c/c
	Land Side	980 KN at 1.219 m c/c

Transfer crane for cargo gear

Number of Crane		32 sets
Rated Load		40 t
Winding Speed	( loaded )	20 m/min
	( no-loaded )	45 m/min
Traveling Speed		70 m/min
Rail Span		23.47 m

Table 2.5 Tolerances for design of traveling rail (for concrete runway)

Check items	Tolerance at installation	Check method	Maintenance tolerance
Straightness	For total length $\leq \pm 50$ mm		By transit $\leq \pm 80$ mm
Span	$\leq \pm 5$ mm for span < 20 m $\leq \pm 10$ mm for span $\geq 20$ m		By steel tape scale (JIS class) $\leq \pm 20$ mm
Height difference between rails	For wheel base length $\leq \text{span}/1000$		By transit $\leq \text{span}/500$
Bend of rail left and right	For 10 m $\leq 10$ mm		By transit For 10 m, $\leq 20$ mm
Inclination	$\leq 1/500$	JC: 1/1000 during installation 1/125 during long term service Measure by transit  Check every 10 m	By transit $\leq 1/250$ or 0.4%

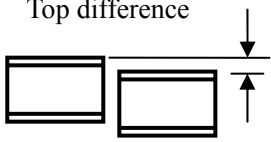
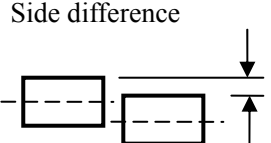
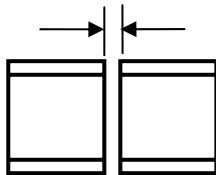
Joint difference	For both top and side $\leq 0.5$ mm	<p>Top difference</p>  <p>Side difference</p> 	By steel scale (JIS class 1)	$\leq 1$ mm
Joint gap (say expansion joint)	$\leq 5$ mm	<p>5 mm during installation 8 mm not contact even in summer</p> 	By steel scale (JIS class 1)	$\leq 7$ mm

Table 2.6 Access bridge

Standard	Container Trailer Load B
Number of Bridge	2 sets
Breadth	One set is 7 m $\times$ 1, the other set 14 m $\times$ 1
Inclination	Not exceeding 2.5 % gradient. Preferably flat.

Based on the requirements and the operating conditions, two possible layouts for the floating container terminal have been proposed by the engineers of Jurong Consultants Pte Ltd (JCPL):

- Option 1—A layout with buildings on the opposite side of the berth to act as counterweight to the quay cranes as shown in Fig. 2.2
- Option 2—A layout without building and the container distributed all over the container terminal as shown in Fig. 2.3.

We focus on option 2 in this study. The floating container terminal is to be constructed from high performance concrete instead of steel due to the following advantages offered by concrete materials:

- high inertia against dynamic motion due to wave actions
- greater fire resistance than steel
- low maintenance cost
- high resistance against fatigue
- cheaper material than steel

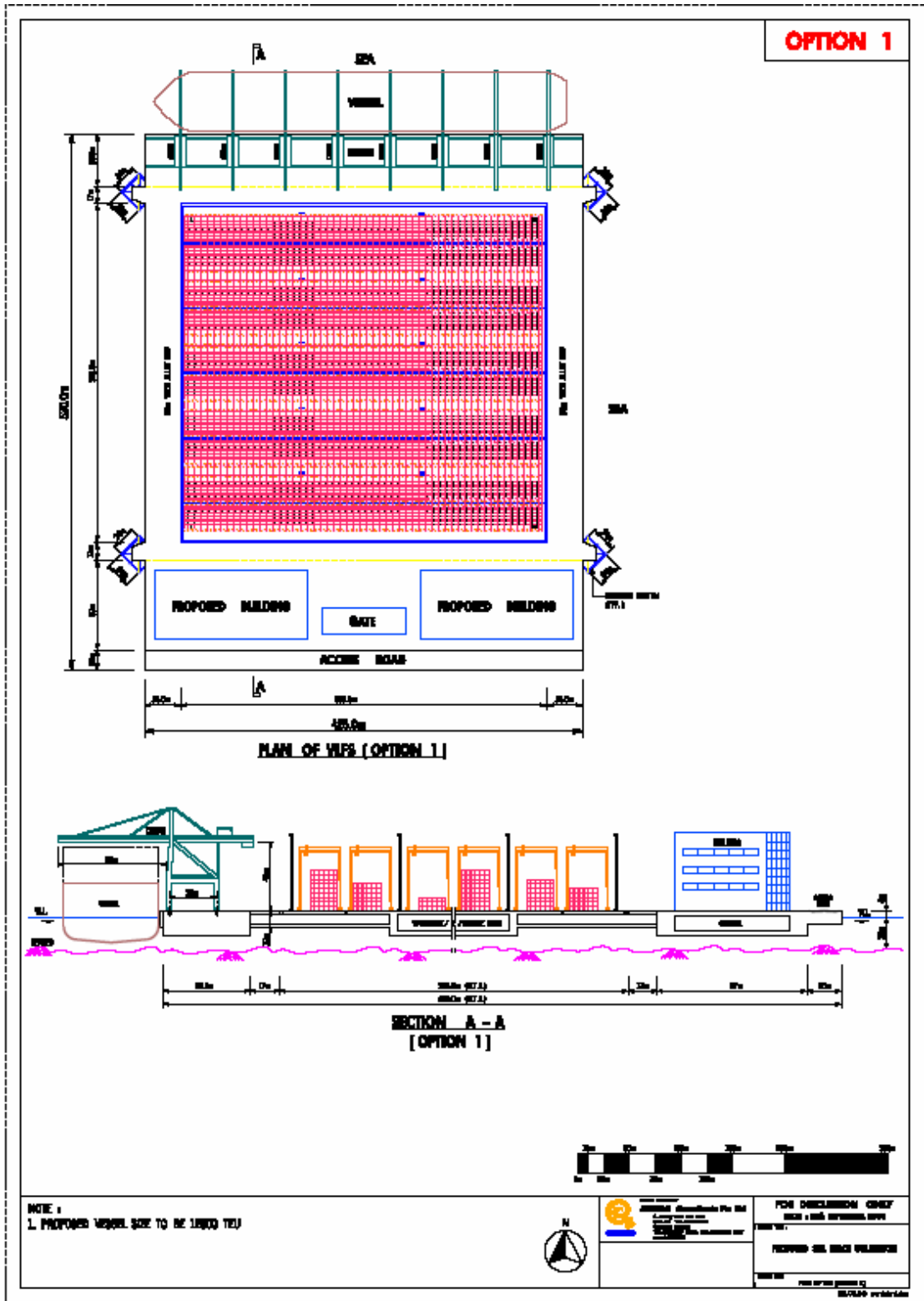


Fig. 2.2 Option 1 layout for very large floating container terminal



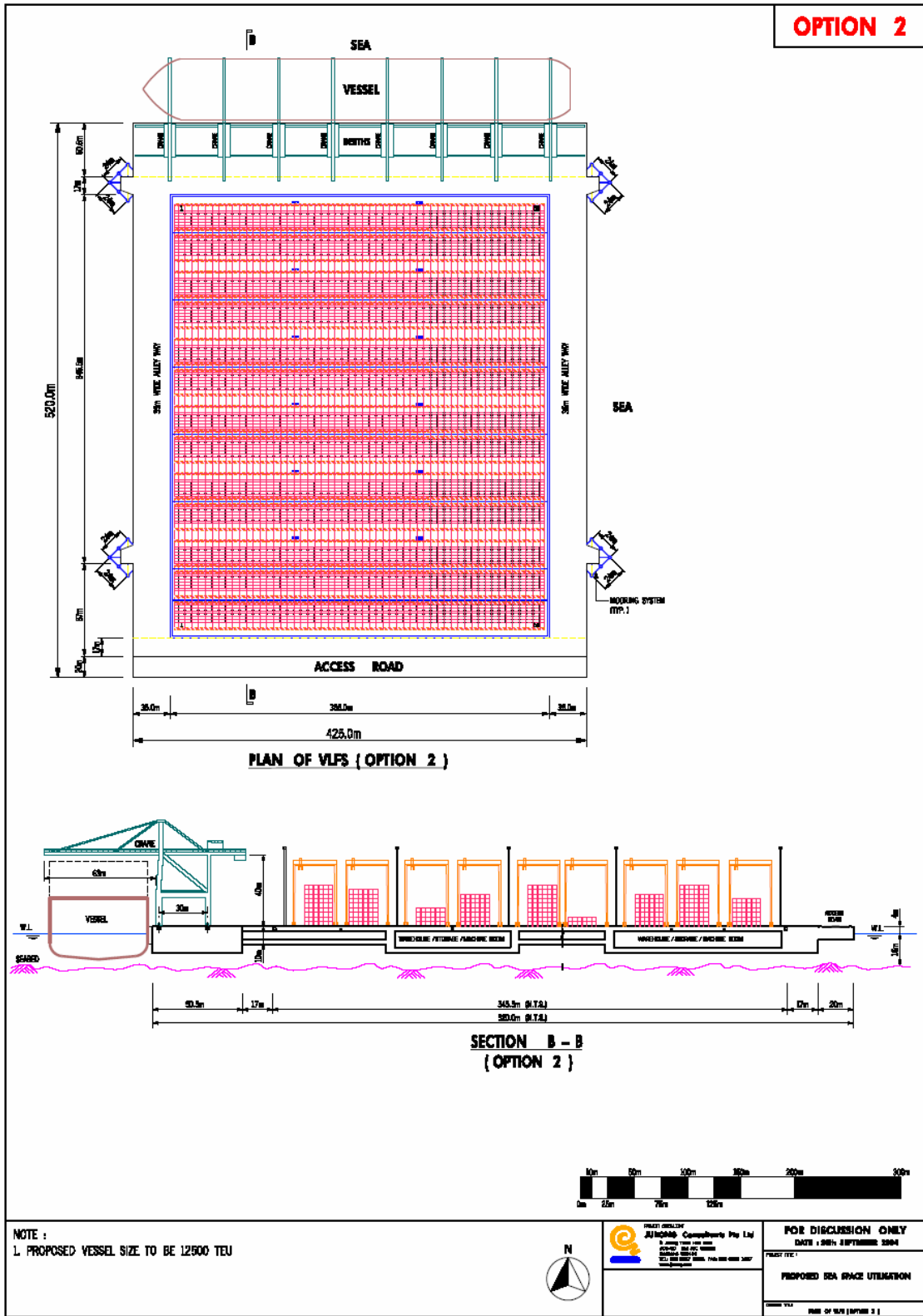
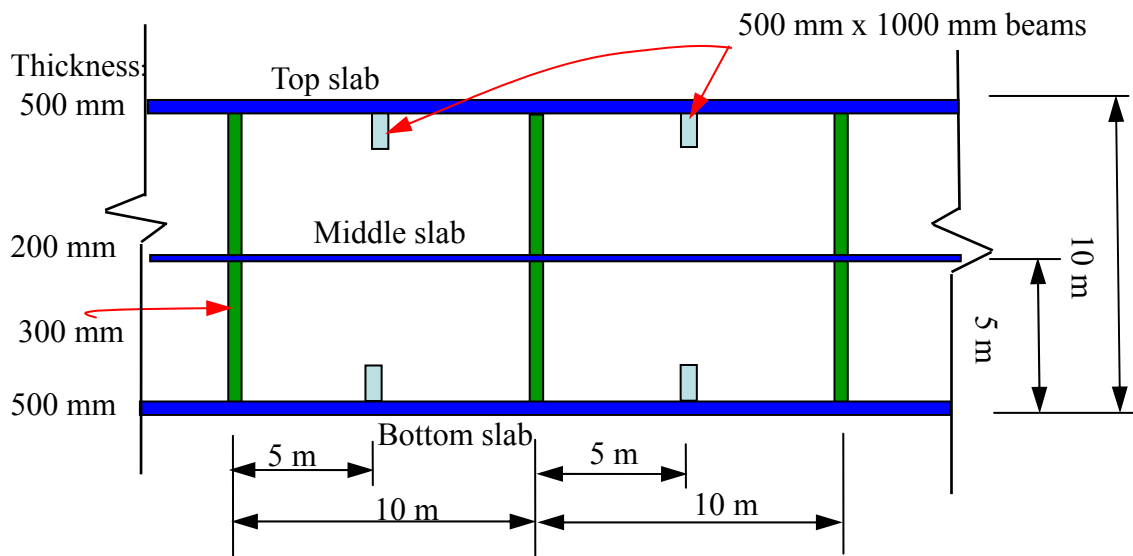


Fig. 2.3 Option 2 layout for very large floating container terminal

Each floating container terminal has a dimension of 470m x 520m x 10m and is made up of 2444 watertight compartments. The interior space of the floating container terminal may be utilized as offices or car parks. Figure 2.4 shows the particular dimensions that associated with a typical watertight compartment in the floating container terminal. The next chapter will deal with the modeling, static analysis of a module of the very large floating container terminal and the detail design of a typical watertight compartment of the module.



*Fig. 2.4 Dimensions of a compartment in floating container terminal*

## **MODELING, STATIC ANALYSIS AND DETAIL DESIGN OF CONTAINER TERMINAL**

### **3.1 Modeling of Floating Container Terminal**

Based on the preliminary sizing and design of the floating container terminal, static analyses are performed to determine the deflection and Mises stresses of the structure under dead and live loads. The finite element software ABAQUS (version 6.6) is adopted for the static analysis. The finite element model for the floating container terminal consists of

- 4-node thin-plate elements (QUAD type: S4R5) for the top, middle and bottom slabs and the vertical walls. The element type “S4R5” means thin shell element with 4 nodes and 5 degrees of freedom. For very large models that will experience only geometrically linear behavior, the linear thin shell element (S4R5) will generally be more cost-effective than the other types of elements. Each element for the slab has dimensions 5m x 5m with a thickness of 0.5m. Each element for the vertical wall has dimensions 5m x 4.8m with a thickness of 0.3m.
- 2-node beam elements (B21) for modeling the beams. Each beam has dimensions of 5m x 1m x 0.5m.
- Elastic springs are attached to the elements of the bottom slab to simulate the

buoyancy forces. The stiffness of the elastic spring is taken as  $250kN/m (= 1.03 \times 10^3 kg/m^3 \times 9.81m/s^2 \times 5m \times 5m)$ .

The total number of elements (plate and beam) is 78407 and the total number of nodes is 78608. The total number of variables used in this finite model is 208287. The finite element model of the floating container terminal is shown in Fig. 3.1. In this model, the structure is made of reinforced concrete with density of  $1900kg/m^3$ , Young's Modulus of 22.9 GPa and Poisson's ratio of 0.2. In the static analysis of the floating container terminal, since the sea state of Singapore is calm, we will not consider the hydro-dynamic effect of the sea water. Thus, the deflection of the structure model is restricted only to the vertical direction.

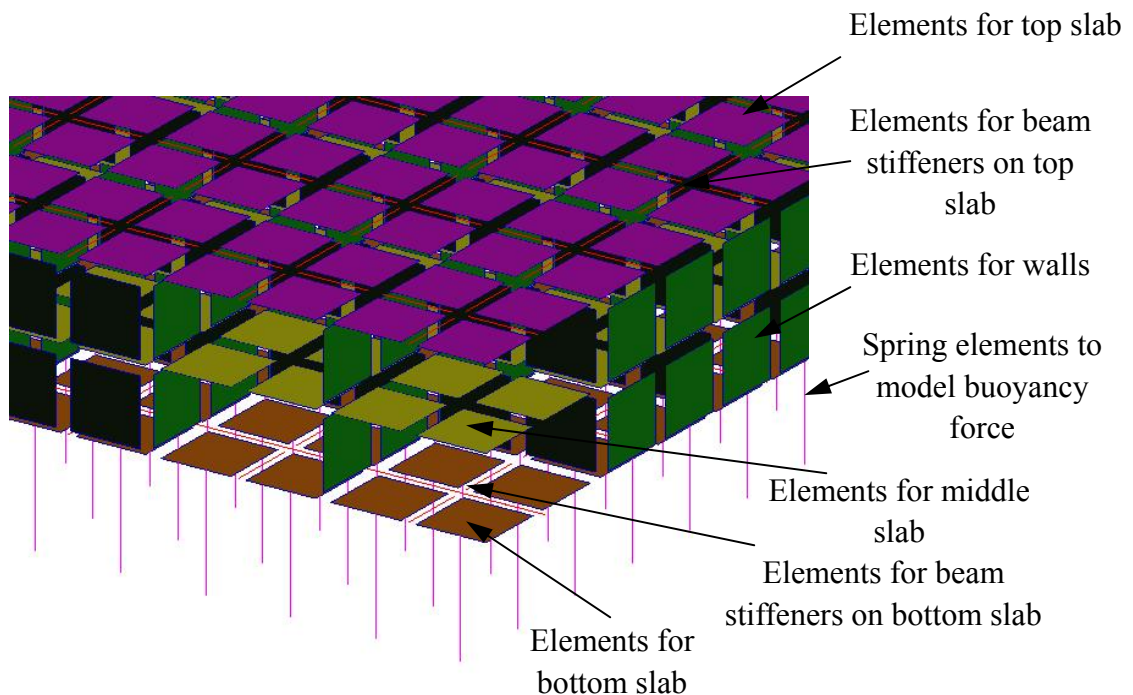


*Fig. 3.1 Finite element model for floating container*

In the following static analysis, three load cases will be considered:

Load Case 1. Self-weight of the floating structure

Load Case 2. Self-weight of the floating structure plus  $50kN / m^2$  uniformly distributed load (equivalent to about 8-tier containers) on the entire top surface  $520m \times 470m$ .

Load Case 3. Self-weight of the floating structure plus  $50kN / m^2$  uniformly distributed load on the central portion  $450m \times 400m$  with no load on the  $35m$  wide road around the perimeter.

### 3.2 Static Analysis of Floating Container Terminal

In the analysis, the principal stresses of the top and bottom slab and deflections of the floating container terminal under the aforementioned loads are obtained. Figure 3.2 shows the deflection contours of the floating structure under 3 load cases and the critical deflection at the corners and the center of the floating structure are given in Table 3.1. It can be seen from Fig. 3.2 and Table 3.1 that the floating structure has negligible differential deflection under load case 1: its own weight and under load case 2: its own weight with distributed load over the entire surface of the floating structure. The between-rail gradient is approximately 0.1% which is well within the limiting value of 0.4%. However, when we have an unloaded 35m wide road round the perimeter of the floating structure (load case 3), we note the significant dishing effect. The differential deflection is about 4.8m, resulting in a between-rail gradient of 1.7%. This will pose problems to the operation of the quay cranes as tilting of the rails is beyond the tolerance of 0.4%.

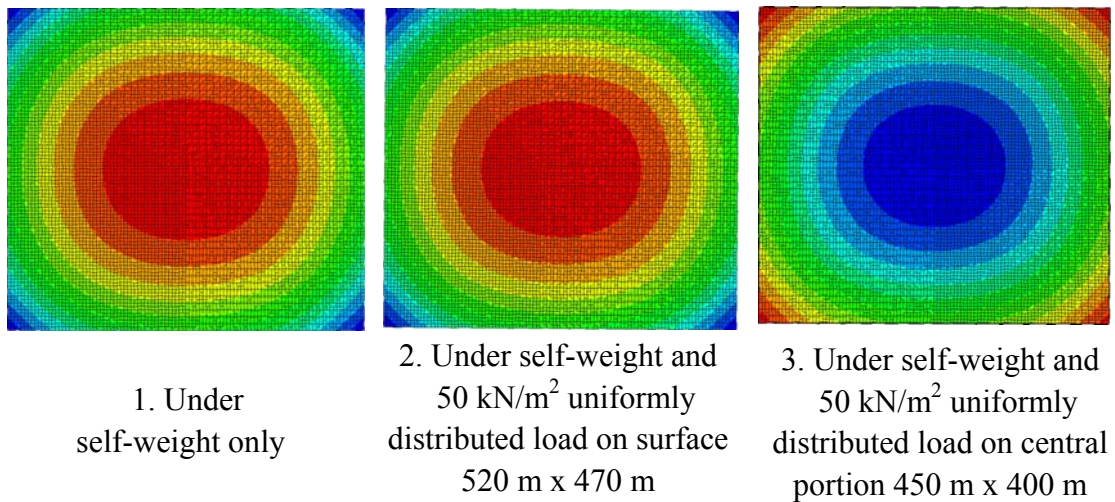


Fig. 3.2 Deflection contours for the three load cases

Table 3.1 Critical deflection of floating structure

Load Cases	Deflection at Corners (m)	Deflection at Centre (m)	Maximum difference in deflections, $\Delta$ (m)	Between Rail Gradient $\delta = \Delta / (\frac{1}{2} \text{structure dimension})$
1	-2.942	-2.814	+0.128	0.1%
2	-8.045	-7.916	+0.129	0.1%
3	-2.920	-7.743	-4.823	1.7%

Figure 3.3 shows the loaded 450m x 400m area of the floating container terminal, the crane loads along the rails. The deflections of the floating structure are computed for various tier numbers of containers in the loaded area. Table 3.2 presents the between-rail gradient and along rail gradient for the quay cranes and yard cranes. It can be seen that the allowable gradient are exceeded when there are three or more tiers of containers. Thus, the quay crane gradients are controlling the design of the floating structure.

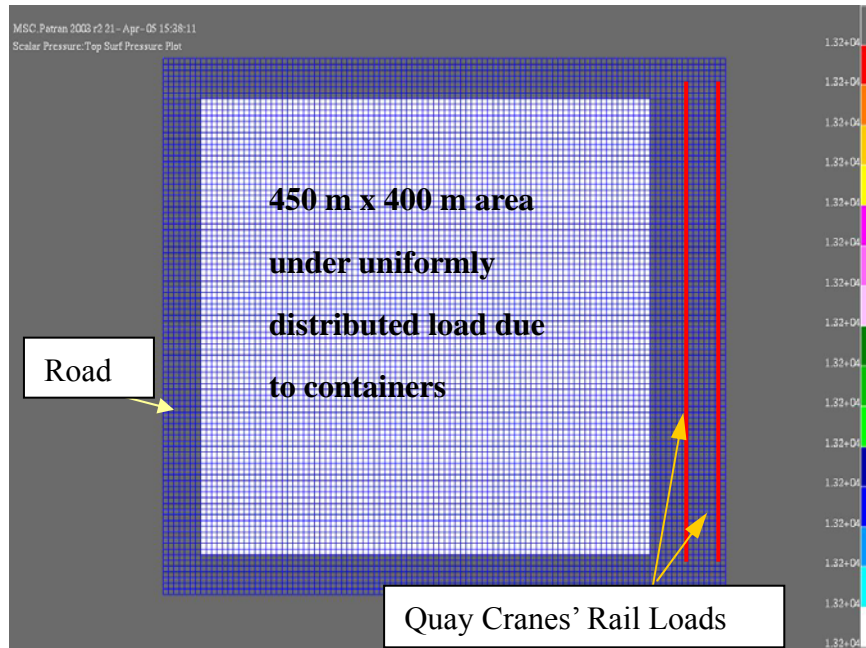


Fig. 3.3 Loaded area of floating container terminal

Table 3.2 Cranes' gradients

Tiers	Gantry crane gradients (%)		Yard Crane gradients (%)
	Between Rails (Transverse direction)	Along Rails (Longitudinal direction)	
0	0.35	0.10	0.35
1	0.10	0.07	0.10
2	0.20	0.20	0.20
3	0.50	0.30	0.30
4	0.85	0.60	0.50
7	1.80	1.40	1.20
Allowable gradients	0.4	0.80	6.0
Gradient Check	The gradients are OK for 0 to 2-tier loading. However, the allowable gradients for the gantry cranes are exceeded when the number of tiers are 3 and above. Thus, the between-rail gradient for quay cranes is the controlling design criterion for the floating structure.		

Table 3.3 presents the principal stresses in the bottom and top slabs of the floating structure. Although the stresses do not satisfy the allowable tensile stresses when there

are three or more tiers of containers, the tensile stresses are not the controlling criterion since reinforcing bars can be used to accommodate the tensile stresses.

*Table 3.3 Principal stresses at top and bottom slab*

Tiers	Uniformly distributed containers' loads (kN/m <sup>2</sup> )	Bottom Slab (MPa)		Top Slab (MPa)	
		Compressive	Tensile	Compressive	Tensile
0	0.	-1.94			+1.83
1	6.610	-1.04			+0.91
2	13.22		+2.06	-1.90	
3	19.82		+3.70	-3.50	
4	26.44		+5.50	-5.17	
7	46.25		+10.5	-10.2	
Allowable stresses		-42	+2.58	-42	+2.58
<b>Stress Check</b>		The stresses are OK for 0 to 2-tier loading but exceed the allowable stresses for 3 or more tiers. However, these stresses can be accommodated by introducing reinforcing bars in the slab.			

The deflections at the corners and center of the floating structure as well as the maximum deflection at the edges are shown in Table 3.4. In order to have a freeboard of 2.5m for the floating container terminal, the allowable deflection is taken as 7.5m. It can be seen that the drafts obtained are acceptable.

*Table 3.4 Deflections and drafts*

Tier	Deflection (m)			Differential Deflection (m)	
	Corner	Edge	Centre	Corner with respect to centre	Edge with respect to centre
0	- 3.53	- 3.06	- 2.89	- 0.64	- 0.17
1	- 3.43	- 3.62	- 3.58	0.15	- 0.04
2	- 3.53	- 3.85	- 4.26	0.73	0.41
3	- 3.53	- 4.27	- 4.95	1.42	0.68
4	- 3.53	- 4.67	- 5.64	2.11	0.97
7	- 3.52	- 5.90	- 7.70	4.18	1.8
Allowable Deflection		-7.5	-7.5		
Draft Check		OK	OK		



### 3.3 Detail Design of a Typical Watertight Cell

In this section, the detail design of a typical watertight compartment of the floating container terminal is to be presented (Wang, Yao and Wee, 2006). The floating container terminal comprises of 2444 cells of 10m x 10m. A cross-section of a typical cell is shown in Fig. 3.4.

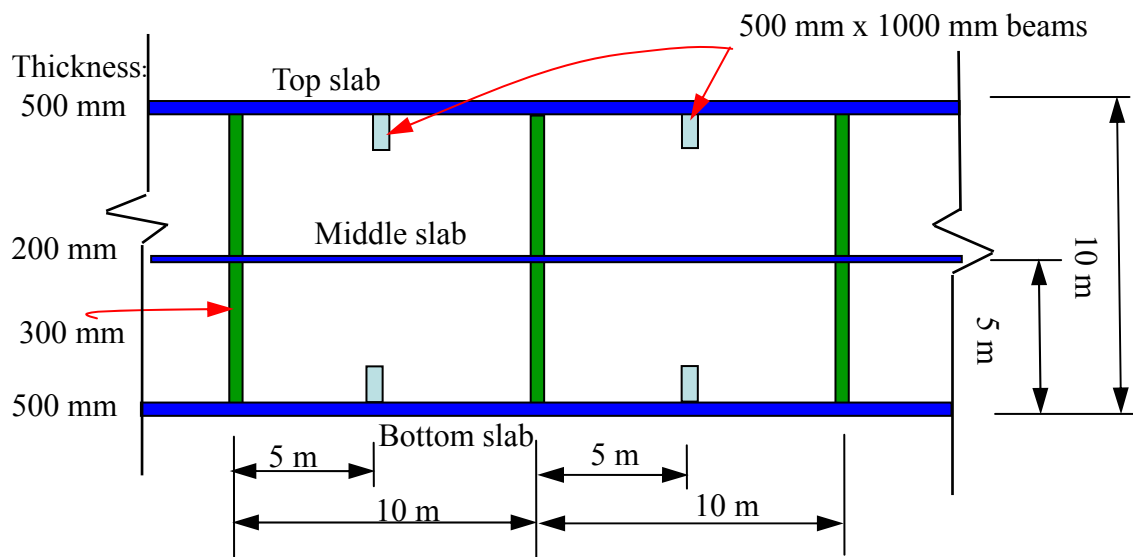


*Fig. 3.4 Compartments of the floating container terminal*

Each cell should be able to carry 7 tiers of containers and each container weighs 30 tons. The dimension of each container is 12.2m x 2.68m. The cell is constructed using high-strength, light-weight, high performance concrete with a density of  $1900\text{kg}/\text{m}^3$  and the reinforcing bars are of steel grade 460. Buoyancy forces also act on the cell.

### 3.3.1 Design of Top Slab

#### 3.3.1.1 Calculation of Bending Moments and Reinforcement Design

As each compartment should be able to carry 7 tiers of containers and each container weighs 30 tons and takes an area of 12.2m x 2.68m, the imposed load  $Q_k$  per unit area due to 7-tier containers is given by

$$Q_k = \frac{30 \times 10^3 \times g \times 7}{12.2 \times 2.68} = 63.0077 \text{ kN} / \text{m}^2 \quad (3.1)$$

The self-weight  $G_k$  per unit area of the concrete cell is given by

$$G_k = 1900 \times 9.81 \times 0.4 = 7.4556 \text{ kN} / \text{m}^2 \quad (3.2)$$

The factored total load to be carried by the cell is therefore given by (BS8110)

$$n = 1.4 \times G_k + 1.6 \times Q_k = 100.14 \text{ kN} / \text{m}^2 \quad (3.3)$$

Based on preliminary calculations to check the crack width control criterion, it was found that the proposed slab thickness of 400mm is not adequate. It is recommended that the slab thickness be increased to 500mm.

From BS8110 Part 1, Table 3.14, the bending moment coefficients  $\beta_s$  for the slab length dimensions  $\lambda_y / \lambda_x = 1$  are given by

$$\beta_{sx} = 0.047 \quad \text{and} \quad \beta_{sy} = 0.045$$

In estimating the cover, we classify the floating structure under “severe” condition. Therefore, from the condition of exposure, BS8110 Part 1-Table 3.2 and 3.3, the nominal concrete cover should be 40mm.

Assuming the adoption of 20mm diameter bars, and the concrete of 40mm, the effective depth  $d$  of the slab is therefore:

$$d = 500 - 40 - 10 = 450 \text{ mm} \quad (3.4)$$

The bending moment  $m_{sx}$  can be calculated by

$$m_{sx} = \beta_{sx} n l_x^2 = 0.047 \times 100.14 \times 5^2 = 117.66 \text{ kNm} / m \quad (3.5)$$

This bending moment will now be used to design the reinforcing bars. To work out the lever arm  $z$ , we first determine the parameter  $K$ .

$$K = \frac{m_{sx}}{f_{cu} b d^2} = \frac{117.66 \times 10^6}{70 \times 1000 \times 450^2} = 0.0083 < 0.156 \quad (3.6)$$

Therefore, the lever arm  $z$  is given by

$$\begin{aligned} z &= d \left[ 0.5 + \left( 0.25 - \frac{K}{0.9} \right)^{1/2} \right] \\ &= 450 \left[ 0.5 + \left( 0.25 - \frac{0.0083}{0.9} \right)^{1/2} \right] \\ &= 445 \text{ mm} > 0.95d = 427 \text{ mm} \end{aligned} \quad (3.7)$$

So we use  $z = 0.95d = 427 \text{ mm}$ . Based on the lever arm, the required area of reinforcing steel  $A_s$  can be calculated from:

$$A_s = \frac{M}{0.95 f_y z} = \frac{117.66 \times 10^6}{0.95 \times 460 \times 427} = 630 \text{ mm}^2 \quad (3.8)$$

So for reinforcing bars in the top slab, we provide 12mm-diameter bars at 125mm spacing between centers which amounts to a total steel area of  $904 \text{ mm}^2 / m$ . Also we provide nominal reinforcement of 10mm-diameter bars at 125mm center to center spacing (with a total steel area of  $628 \text{ mm}^2 / m$ ) at the top side of the top slab. Owing to the symmetry of the compartment, the same area of bars is provided for the other direction of the slab.

### 3.3.1.2 Calculation of Shear Force and Reinforcement Design

From BS8110 Part 1, Table 3.14, the shear force coefficients  $\beta_v$  for the slab length dimensions  $\lambda_y / \lambda_x = 1$  are given by:

$$\beta_{vx} = \beta_{vy} = 0.40 \quad (3.9)$$

The shear force

$$V_{sx} = \beta_{vx} n l_x = 0.4 \times 100.14 \times 5 = 200.3 \text{ kN} \quad (3.10)$$

Thus, the shear stress is

$$v = \frac{V_{sx}}{bd} = \frac{200.3 \times 10^3}{1000 \times 450} = 0.445 \text{ N/mm}^2 \quad (3.11)$$

In the meantime, due to the dimension of the slab and property of the material, we can get design ultimate shear stress  $v_c$  from

$$\begin{aligned} v_c &= \frac{0.79 \left( 100 \frac{A_s}{bd} \right)^{1/3} \left( \frac{400}{d} \right)^{1/4}}{\gamma_m} \times \left( \frac{f_{cu}}{25} \right)^{1/3} \\ &= \frac{0.79 \left( 100 \frac{678}{1000 \times 450} \right)^{1/3} \left( \frac{400}{450} \right)^{1/4}}{1.25} \times \left[ \frac{40}{25} \right]^{1/3} = 0.3819 \end{aligned} \quad (3.12)$$

where  $\gamma_m$  is the partial factor for material strength. From BS8110 Part 1-Table 2.2,  $\gamma_m = 1.25$ ;  $f_{cu}$  is the characteristic strength of the concrete, and it cannot be larger than 40 in the formula. As  $v > v_c$ , shear reinforcement is required.

From BS8110 Part 1-Table 3.16, when  $v_c < v < v_c + 0.4$ , the form of shear reinforcement to be provided is “minimum links in areas where  $v > v_c$ ”. Therefore the area of shear reinforcement to be provided is given by

$$A_{sv} \geq \frac{0.45 b s_v}{0.95 f_{yv}}$$

where  $s_v$  is the spacing of links and  $f_{yv}$  is the characteristic strength of link

reinforcement. By adopting 10mm diameter links  $A_{sv} = 157mm^2$  and

$$s_v = \frac{0.95 f_{yv} A_s}{0.4b} = \frac{0.95 \times 460 \times 157}{0.4 \times 1000} = 171.5mm \leq 0.75d = 0.75 \times 340 = 255mm \quad (3.13)$$

So for the reinforcing bars for shear resistance, we provide 10mm links at 150mm spacing between centers which amounts to a total steel area of  $157mm^2 / m$ .

### 3.3.1.3 Deflection Control

For the top slab, the span/effective depth ratio is  $5000/450 = 11.1$ . From BS8110 Part 1-Table 3.9, the span/effective depth ratio for this condition is 26. We also have to include the modification factors. From BS8110 Part 1-Table 3.10, the modification factor for tension reinforcement may be obtained from the following formula:

$$0.55 + \frac{(477 - f_s)}{120(0.9 + \frac{M}{bd^2})} \leq 2.0 \quad (3.14)$$

where  $f_s$  is the estimated design service stress in the tension reinforcement and may be taken as  $2f_y/3 = 2 \times 460/3 = 307$ . So the first modification factor is 1.51. Another modification factor to be considered may be obtained from the formula:

$$100 \frac{A_{sprov}}{bd} = 100 \times \frac{628}{450 \times 1000} \approx 0.14 \quad (3.15)$$

From BS8110 Part 1-Table 3.11, the factor is 1.05. As the modification factor is considered, the deflection is satisfied.

### 3.3.1.4 Crack Control

The crack may be assumed to exist at the center of the bars as shown in Fig. 3.5.

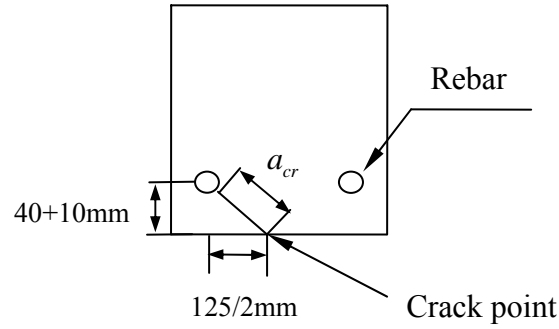


Fig. 3.5 Position that crack may occur

The distance from the cracking point to the nearest bar  $\alpha_{cr}$  is obtained from

$$\alpha_{cr} = \sqrt{(40+6)^2 + \left(\frac{125}{2}\right)^2} - 6 = 71.6\text{mm} \quad (3.16)$$

The area of tension steel relative to concrete in a section  $\rho$  is obtained from

$$\rho = \frac{A_{st}}{bd} = \frac{904}{1000 \times 450} = 0.002 \quad (3.17)$$

where  $A_{st}$  is the area of steel in tension.

The area of compression steel relative to concrete in a section  $\rho_1$  is obtained from

$$\rho_1 = \frac{A_{sc}}{bd} = \frac{628}{1000 \times 450} = 0.0014 \quad (3.18)$$

where  $A_{sc}$  is the area of steel in compression.

The modular ratio  $\alpha_e$  is obtained from

$$\alpha_e = \frac{E_s}{E_c} = \frac{200}{11.45} = 17.467 \quad (3.19)$$

where  $E_s$  and  $E_c$  are the modulus of elastic of steel and concrete respectively.

To determine the neutral axis depth  $x$ , we have to obtain  $x/d$  through the formula

$$\frac{x}{d} = -(\rho + \rho_1)\alpha_e + \left( ((\rho + \rho_1)\alpha_e)^2 + 2\left(\rho_1 \frac{d_1}{d} + \rho\right)\alpha_e \right)^{0.5} = 0.221 \quad (3.20)$$

Then  $x$  is calculated as  $x = d \times \frac{x}{d} = 99.4$

In order to obtain the second moment of area  $I$ , we have to evaluate  $I/bd^3$  by

$$\frac{I}{bd^3} = \frac{(x/d)^3}{3\alpha_e} + \rho_1 \left( \frac{d_1}{d} - \frac{x}{d} \right)^2 + \rho \left( 1 - \frac{x}{d} \right)^2 = 1.445E-3 \quad (3.21)$$

Then  $I$  is calculated as  $I = bd^3 \times 1.445 \times 10^{-3} = 1.317 \times 10^8$

To determine the crack width, we also need to calculate the average strain  $\varepsilon_m$

through the formulas 3.22 to 3.26:

$$f_s = \frac{M_s(d-x)}{I} \quad (3.22)$$

$$\varepsilon_s = \frac{f_s}{E_s} \quad (3.23)$$

$$\varepsilon_1 = \frac{\varepsilon_s(h-x)}{(d-x)} \quad (3.24)$$

$$\varepsilon_t = \frac{-b(h-x)^2}{3E_s A_{st}(d-x)} \quad (3.25)$$

$$\varepsilon_m = \varepsilon_1 + \varepsilon_t \quad (3.26)$$

Then, the crack width is calculated using the formula

$$w_d = \frac{3\alpha_{cr}\varepsilon_m}{\left( 1 + \frac{2(\alpha_{cr}-c)}{h-x} \right)} = 0.255mm \quad (3.27)$$

Since the width of the crack is less than 0.3mm, crack control check is OK.

### 3.3.2 Design of Middle Slab

#### 3.3.2.1 Calculation of Bending Moments and Reinforcement Design

If the compartment of the floating container terminal is to be used as a car park, we have to consider the load of the cars when designing the middle slab. In general, the dimension of a car is 2m by 6m, and the self-weight of a car is 2500kg. Thus, the load per unit area is:

$$Q_k = \frac{2500 \times 9.81}{2 \times 6} = 2.044 \text{ kN} / \text{m}^2 \quad (3.28)$$

We can design the middle slab in the same way as the top slab, noting the difference in loading magnitude and the thickness of the middle slab which is 200mm.

The self-weight per unit area of the middle slab is

$$G_k = 1900 \times 9.81 \times 0.2 = 3.728 \text{ kN} / \text{m}^2 \quad (3.29)$$

Then the factored total load to be carried by the middle slab is given by

$$n = 1.4 \times G_k + 1.6 \times Q_k = 1.4 \times 3.728 + 1.6 \times 2.044 = 8.5 \text{ kN} / \text{m}^2 \quad (3.30)$$

From BS8110 Part 1, Table 3.14, the bending moment coefficients  $\beta_s$  for the slab length dimensions  $\lambda_y / \lambda_x = 1$  are given by

$$\beta_{sx} = 0.055 \quad \text{and} \quad \beta_{sy} = 0.056$$

By assuming that 10mm diameter bars will be used and the cover is 30mm, the effective depth  $d$  of the slab is thus given by

$$d = 200 - 30 - 5 = 165 \text{ mm} \quad (3.31)$$

The moments can be calculated from

$$m_{sx} = \beta_{sx} n l_x^2 = 0.055 \times 8.5 \times 10^2 = 46.75 \text{ kNm} / \text{m} \quad (3.32)$$

In order to determine the lever arm  $z$ , we first determine the parameter  $K$



$$K = \frac{m_{sx}}{f_{cu}bd^2} = \frac{46.75 \times 10^6}{70 \times 1000 \times 165^2} = 0.0245 < 0.156 \quad (3.33)$$

Therefore, the lever arm  $z$  is given by

$$z = d \left[ 0.5 + \left( 0.25 - \frac{K}{0.9} \right)^{1/2} \right] = 165 \left[ 0.5 + \left( 0.25 - \frac{0.0245}{0.9} \right)^{1/2} \right] \quad (3.34)$$

$$= 160mm > 0.95d = 156.75mm$$

So we use  $z = 0.95d = 156.75mm$ .

Based on the lever arm, the required area of reinforcing steel  $A_s$  can be calculated from

$$A_s = \frac{M}{0.95f_y z} = \frac{46.75 \times 10^6}{0.95 \times 460 \times 156.75} = 682mm^2 \quad (3.35)$$

So for the reinforcing bars in the middle slab, we provide 14mm diameter bars at 200mm spacing between centers which amounts to a total area of  $769mm^2 / m$ . Also we provide nominal reinforcement of 10mm diameter bars at 125mm center to center spacing at the top of the slab to give an area of  $628mm^2 / m$ .

### 3.3.2.2 Calculation of Shear Force and Reinforcement Design

From BS8110 Part 1, Table 3.15, we can calculate the shear force coefficients for the slab with the dimension  $l_y / l_x = 1$

$$\beta_{vx} = \beta_{vy} = 0.33$$

Then the shear force can be calculated by

$$V_{sx} = \beta_{vx} nl_x = 0.33 \times 8.5 \times 10 = 28.05kN \quad (3.36)$$

Thus, the shear stress  $\nu$  is obtained from

$$\nu = \frac{V_{sx}}{bd} = \frac{28.05}{1000 \times 165} = 0.17N / mm^2 \quad (3.37)$$

The design ultimate shear stress  $v_c$  is calculated as

$$v_c = \frac{0.79 \left( 100 \frac{A_s}{bd} \right)^{1/3} \left( \frac{400}{d} \right)^{1/4}}{\gamma_m} \times \left( \frac{f_{cu}}{25} \right)^{1/3} \quad (3.38)$$

$$= \frac{0.79 \left( 100 \frac{769}{1000 \times 165} \right)^{1/3} \left( \frac{400}{165} \right)^{1/4}}{1.25} \times \left[ \frac{40}{25} \right]^{1/3} = 0.715$$

As  $v < v_c$ , shear reinforcement is not required.

### 3.3.2.3 Deflection Control

In this condition, the span/effective ratio is  $10000/165 = 60$ . Referring to BS8110 Part 1, Table 3.9 and Table 3.10, we have to either increase the thickness of the slab or add compression bars in the upper area of the slab so as to satisfy the span/effective depth ratio. We choose to increase the thickness of the slab.

By assuming the thickness of the middle slab to be 300mm, the effective depth is 265mm. Thus, the span/effective depth ratio is  $10000/265 = 37.7$ . We can get the first modification factor from

$$0.55 + \frac{477 - f_s}{120 \left( 0.9 + \frac{M}{bd^2} \right)} = 1.45 \leq 2.0 \quad (3.39)$$

The second modification factor is 1.08 as

$$100 \frac{A'_{sprov}}{bd} = 100 \times \frac{628}{265 \times 1000} \approx 0.25 \quad (3.40)$$

Thus, the span/effective depth ratio is calculated as

$$26 \times 1.45 \times 1.08 = 40.7 > 37.7 \quad (3.41)$$

The span/effective depth ratio is thus acceptable.

### 3.3.2.4 Crack Control

The crack width is found to be 0.156mm which is less than 0.3mm, so it is satisfactory.

### 3.3.3 Design of Bottom Slab

The load on the bottom slab is the same as the load on the middle slab, but for the bottom slab, we have to consider the buoyancy force of the sea water which is determined by the total load of the container terminal. We provide beam stiffeners in the bottom slab, just like we do for the top slab.

To be conservative, we neglect the downward load on the bottom slab. This means that we could consider the bottom slab to be subjected to the same load as the top slab except that the load direction is reverse as the bottom slab is subjected to buoyancy force. So for the reinforcing bars in the bottom slab, we provide 12mm diameter bars at 125mm spacing between centers at the top side that amounts to an area of  $904\text{mm}^2 / \text{m}$ . Also we provide a nominal reinforcement of 10mm diameter bars at 125mm between center to center at the bottom side of the bottom slab to give an area of  $628\text{mm}^2 / \text{m}$ . Figure 3.6 shows the reinforcement details for a typical unit compartment.

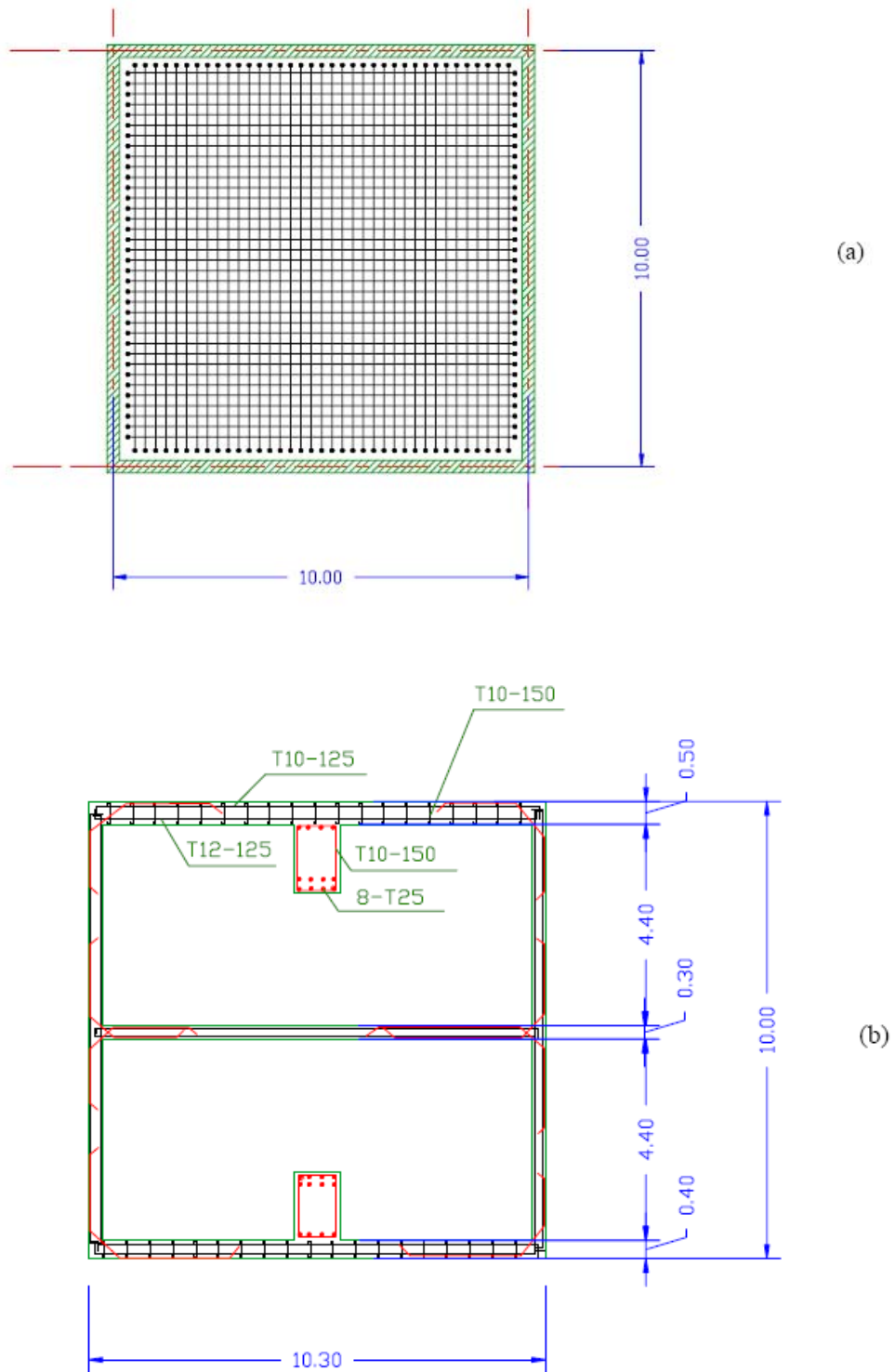


*Fig. 3.6 (a) Plan view and (b) side view of the cell with reinforcement details  
(All dimensions are in meters)*

### 3.3.4 Design of Vertical Walls

Owing to the symmetry of the compartment, each wall will carry a quarter of the loading transmitted from the slab and their self-weight. As the compartments are exposed to the water, the water pressure is added to the loading on the wall as shown in Fig. 3.7.

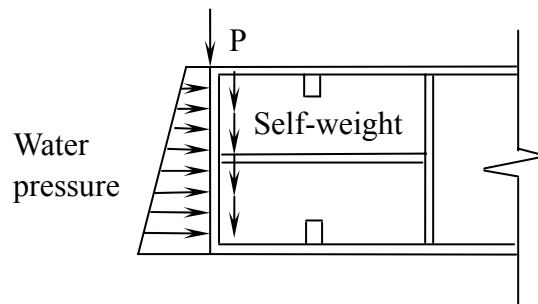


*Fig. 3.7 Loading condition of the compartment walls*

#### 3.3.4.1 Type of Wall-Slenderness

The wall is 300mm thick and braced. Referring to Table 3.19 in the code, the end conditions are as follows:

1. At the top of the wall is connected to a slab 500 deep, i.e. condition 1;
2. At the bottom the connection to the bottom slab is designed to carry moment, i.e. condition 1.

From Table 3.19, the effective height factor  $\beta$  is 0.75. The clear height is 4400mm.

The slenderness  $\delta$  is thus given by

$$\delta = 0.75 \times 4400 / 300 = 11 < 15 \quad (3.42)$$

The wall is 'stocky' since the slenderness is less than 15.

### 3.3.4.2 Dead and Imposed Loads on Wall

The self-weight of the wall is calculated as follows:

$$\text{Density of the wall is } 1900 \text{ kg} / \text{m}^3 \times 9.81 = 18.639 \text{ kN} / \text{m}^3 \quad (3.43)$$

Thus, the characteristic self-weight is  $10 \times 1 \times 0.3 \times 18.639 = 55.9 \text{ kN}$  and the design self-weight is  $55.9 \times 1.4 = 78.3 \text{ kN}$ .

The load transmitted from the top slab is given by

$$P = \frac{1}{4}(Q_k + G_k) \times 10^2 = \frac{1}{4}(63.0077 + 7.4556) \times 10^2 / 10 = 176.16 \text{ kN} \quad (3.44)$$

By ignoring the water pressure firstly, the total design load is obtained

$$N = 176.16 + 78.3 = 254.46 \text{ kN} \quad (3.45)$$

From BS8110 Part 1, Clause 3.8.4.4

$$N = 0.35 f_{cu} A_c + 0.7 A_{sc} f_y \quad (3.46)$$

Thus, the concrete is sufficient to resist the axial force and so there is no need to provide reinforcing bars in the walls.

### 3.3.4.3 Corresponding Design Due to Water Pressure

#### A. Calculation of Bending Moment and Reinforcement Design

The draft of the container is assumed to be 5m (which will be the case in most operating conditions). For the perimeter walls below the water, we can consider it as a vertical slab (of height 5m and unit length) under hydrostatic force (varying from zero value at the water surface to  $q$  at the bottom surface). The above method will be used to design the reinforcement for these perimeter walls. Considering simply supported edges for the vertical slab panel unit, the maximum moment is given by

$ql^2 / 15.625$  (Young and Budynas, 2002). For this situation,  $q$  is  $10kN/m$  and  $l$  is  $5m$ . Thus, the maximum moment is  $80kNm$ .

The lever arm  $z$  is calculated as

$$z = d \left[ 0.5 + \sqrt{0.25 - \frac{K}{0.9}} \right] \quad (3.47)$$

where  $d$  is the effective thickness of the slab and the parameter  $K$  can be obtained from

$$K = \frac{M}{f_{cu} b d^2} = \frac{80 \times 10^6}{70 \times 1000 \times 250^2} = 0.0183 < 0.156 \quad (3.48)$$

Therefore

$$z = 245mm > 0.95d = 237.5mm \quad (3.49)$$

So we use

$$z = 0.95d = 237.5mm$$

Then the area of reinforcement is given by

$$A_s = \frac{M}{0.95 f_y z} = \frac{80 \times 10^6}{0.95 \times 460 \times 237.5} = 771mm^2 \quad (3.50)$$

So for the reinforcement of the walls, we provide 14mm diameter bars at 125mm spacing between centers, which amounts to a total area of  $1230mm^2 / m$ . In the mean time, we provide 10mm diameter bars at 125mm center to center spacing to give an area of  $628mm^2 / m$  for the nominal reinforcement.

B. Calculation of Shear Force and Reinforcement Design

$$V_{sx} = \frac{7}{16} ql = \frac{7}{16} \times 50 \times 5 = 109.38kN \quad (3.51)$$

$$v = \frac{V_{sx}}{bd} = \frac{109.38 \times 10^3}{1000 \times 450} = 0.243 \quad (3.52)$$

$$\begin{aligned}
v_c &= \frac{0.79 \left(100 \frac{A_s}{bd}\right)^{1/3} \left(\frac{400}{d}\right)^{1/4}}{\gamma_m} \times \left(\frac{f_{cu}}{25}\right)^{1/3} \\
&= \frac{0.79 \left(100 \frac{791}{1000 \times 250}\right)^{1/3} \left(\frac{400}{250}\right)^{1/4}}{1.25} \times \left[\frac{40}{25}\right]^{1/3} = 0.5665
\end{aligned} \tag{3.53}$$

As  $v < v_c$ , no shear reinforcement is required.

### C. Deflection Control

The span/effective depth ratio is  $5000/450 = 11.1$ . From BS8110 Part 1, Table 3.10, the span/effective depth ratio is 26. We can get the first modification factor from

$$0.55 + \frac{(477 - f_s)}{120 \left(0.9 + \frac{M}{bd^2}\right)} = 1.2 \leq 2.0 \tag{3.54}$$

The second modification factor is 1.05 as

$$100 \frac{A'_{sprov}}{bd} = 100 \times \frac{628}{450 \times 1000} \approx 0.14 \tag{3.55}$$

Since the modification factors are considered, the deflection is satisfied.

### D. Crack Control

The crack width is found to be 0.254mm which is less than 0.3mm, so it is satisfactory.



### 3.3.5 Design of Beam Stiffeners for Top Slab

As the bending moment is large and the crack exceeds the permission, we have to put beam in the top slab to help to resist the moment. The cross-section of the beam has to be increased to 1000mm x 1500mm to resist the shear force and to control the crack width. So the effective depth of the beam is 1460mm and the width is 1000mm.

#### 3.3.5.1 Calculation of Stress Resultants and Reinforcement Design

Through calculation, we can obtain that the area of bars needed in the tension area is  $A_s = 3610mm^2$ . Thus, we provide 8 rebar of 25mm diameter to give an area of  $3927mm^2/m$ . We also provide 4 rebar of 12mm diameter to be the nominal reinforcement.

We also could obtain that  $\nu > \nu_c$ . Thus, shear reinforcement is needed. We choose to adopt 10mm diameter links, i.e.

$$A_{sv} = 157mm^2$$

$$S_v = \frac{0.95f_{yv}A_s}{0.4b} = \frac{0.95 \times 460 \times 157}{0.4 \times 1000} = 171.5mm \leq 0.75d \quad (3.56)$$

So we provide 10mm links at 150mm between centers in the beam.

#### 3.3.5.2 Deflection Control

Considering the modification factors, the deflection is satisfied.

### **3.3.5.3 Crack Control**

The crack width is found to be 0.19mm which is less than 0.3mm, so it is satisfied.

### **3.3.6 Design of Beam Stiffeners for Bottom Slab**

In order to increase the stiffness of the whole structure, we also have to add beams as shown in Fig. 3.6. The beams have cross-section dimensions of 1000mm x 1500mm with 8 rebar of 25mm diameter to give an area of  $3927\text{mm}^2/m$ . The nominal reinforcement is 4 rebar of 12mm diameter. The reinforcements are placed at the top of the bottom slab as shown in Fig. 3.6.

# **CONTROLLING DESIGN CRITERION AND GILL CELL CONCEPT**

## **4.1 Introduction**

In the static analysis of Chapter 3, it can be seen that the drafts are larger than the allowable limit of 2.5m (see Table 3.4). Though the allowable principal tensile stresses are exceeded when 3 or more tiers are loaded (see Table 3.3), one can introduce reinforcing bars to cater for the tensile stresses. However when the stacking yard is loaded by 3-tier of containers or more, the allowable quay crane gradient is exceeded (see Table 3.2). Thus, the between-rail gradient for quay cranes is the controlling design criterion for the floating structure. This undesirable “dishing effect” must be overcome for smooth operation of the container terminal, especially when the terminal is fully loaded with containers.

In this chapter, the novel gill cells concept (Wang et al., 2006) is introduced so as to minimize the dishing effect, i.e., to reduce the differential deflection between the central portion and corners of the floating structure.

## **4.2 The Concept of Gill Cells**

There are a few ways to decrease the dishing effect or the differential deflection. One solution is to increase the flexural stiffness of the structure by increasing the depth

of the floating structure and the thickness of the top and bottom slabs. This solution leads to an increase in costs. Another solution is to increase the height of the central portion of the floating structure in order to increase the flexural stiffness of the structure.

Here, we present an alternative solution for the problem. The solution involves perforating the bottom surface of the perimeter compartments (or cells) to allow sea-water to freely flow in and out. By so doing, the perforated cell region has zero buoyancy. The elimination of buoyancy force at the edges of the floating structure simulates “hogging moments” at the edges. The hogging moments bend the edges of the structure backwards and due to the flexural rigidity of the structure, the central portion gets lifted up. The overall effect is a flatter surface. Note that the floating structure maintains its structural stiffness integrity since the holes or slits made are small.

Wang et al. (2006) refer these perforated cells as “gill cells”. Figure 4.1 shows a cross-sectional portion of a floating structure with gill cells while Figure 4.2 shows examples of shapes and locations of the slits/holes for the gill cells. Apart from the gill cell region of the floating structure, we have buoyancy force acting on the bottom surface of the structure. By adjusting the number and location of gill cells, the floating container terminal surface can be kept as flat as possible under varying loadings due to changing tiers of containers. Figure 4.3 shows the proposed locations of the gill cells when the container terminal is loaded with 5-7 tiers of containers. Figures 4.4 and 4.5 show the side view and plan view of the floating container terminal with gill cells. At

the gill cell locations, the elastic spring attached to the bottom surface of the structure model are removed as there are no buoyancy forces.

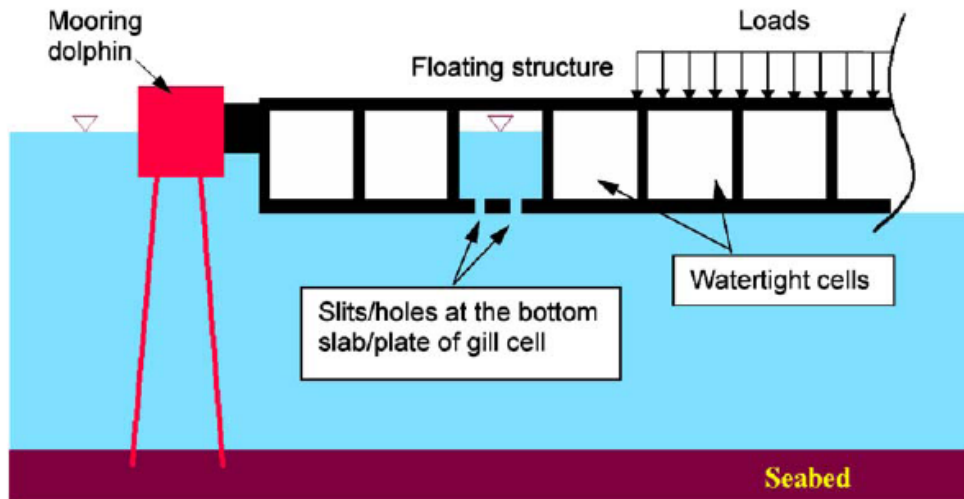


*Fig. 4.1 Cross-sectional portion of the floating structure with gill cells*

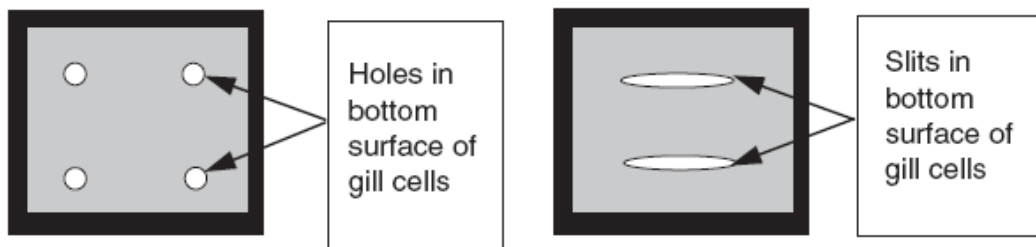


*Fig. 4.2 Examples of shapes and locations of slits/holes for gill cells*

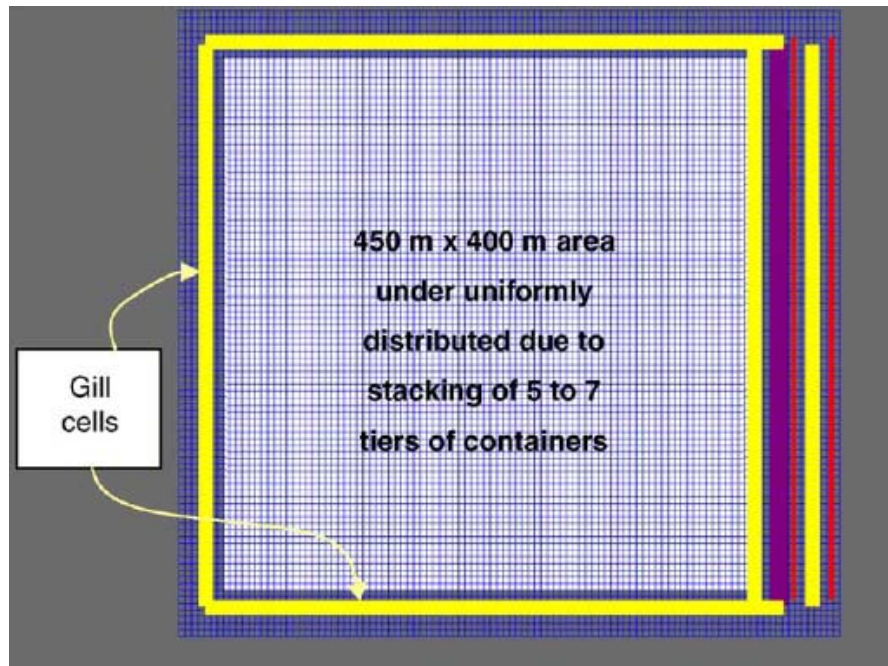


*Fig. 4.3 Proposed location of gill cells when floating structure is loaded in the center portion*

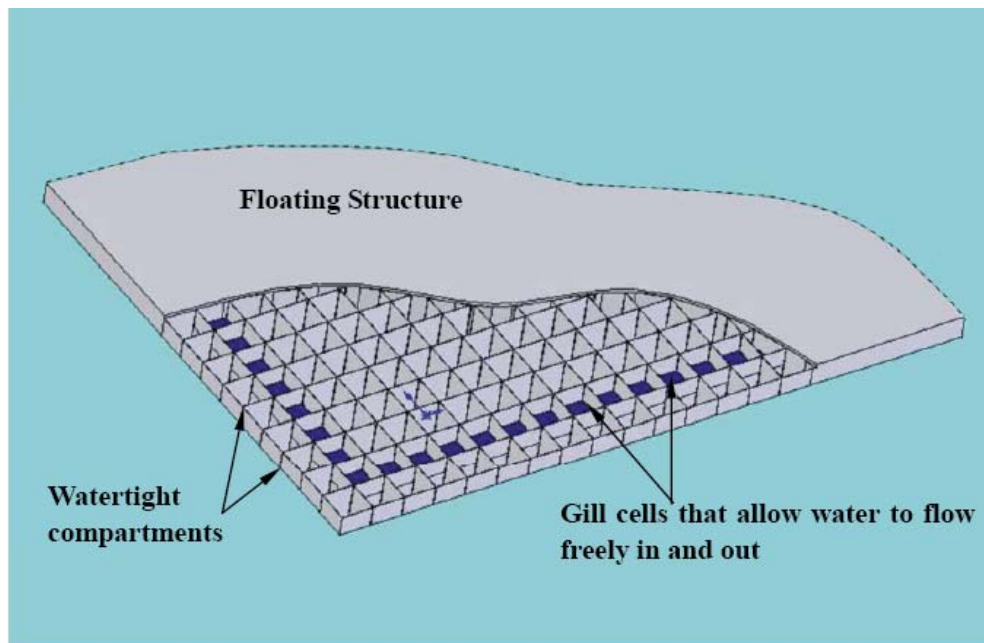


*Fig. 4.4 Side view of floating structure*

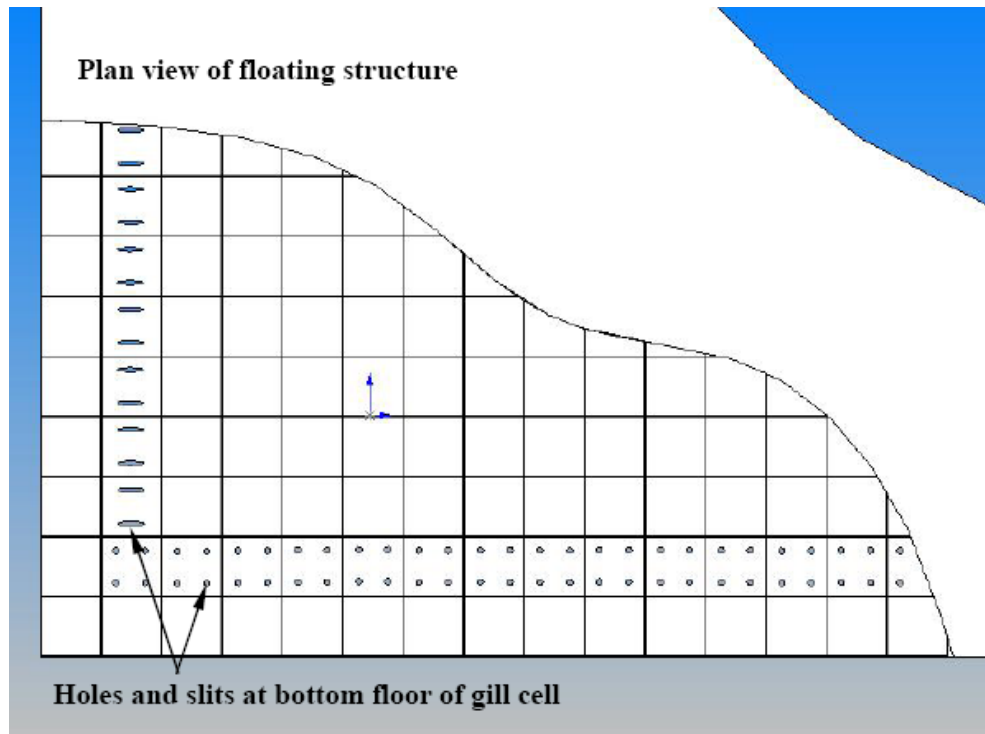


*Fig. 4.5 Plan view of floating structure*

### 4.3 Effect of Gill Cells

Finite element analyses were performed on the floating structure with gill cells. Results of the quay crane rail gradient, major principal stresses and the drafts of the floating structure are shown in Tables 4.1, 4.2 and 4.3, respectively. Compared to the analyses results without gill cells (see Tables 3.2 to 3.4), it can be seen that when a very large floating structure is loaded heavily in its central portion, the gill cells provide an effective solution to mitigate the differential deflection. In addition, the bending stresses are reduced since the curvature of the floating structure is decreased. Figures 4.6 and 4.7 show the deflection and stress contours for floating structures under 7-tier container loading, crane load and self-weight with and without gill cells.

Table 4.1 Crane gradient with gill cells

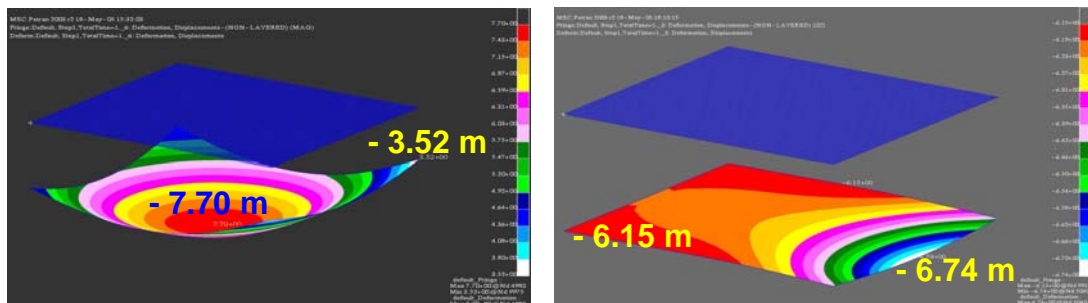
Tiers of Container	Quay crane gradients (%)		Yard crane gradient (%)
	Between rails	Along rails	
5	0.25	0.2	0.25
6	0.1	0.3	0.3
7	0.2	0.25	0.25
Allowable gradients	0.4	0.8	6.0

Table 4.2 Principal stresses at top and bottom slabs with gill cells

Tiers	Uniformly distributed containers' loads (kN/m <sup>2</sup> )	Bottom Slab (MPa)		Top Slab (MPa)	
		Compressive	Tensile	Compressive	Tensile
5	33.04	-1.35			+1.12
6	39.66		1.76	-1.69	
7	46.25		2.30	-2.23	
Allowable stresses		-42	+2.58	-42	+2.58

Table 4.3 Deflection and drafts with gill cells

Tier	Deflections (m)			Difference in deflections	
	Corner	Edge	Centre	Corner to centre (m)	Edge to centre (m)
5	-6.15	-6.74	-6.27	0.12	-0.47
6	-6.48	-7.02	-6.93	0.45	-0.09
7	-6.69	-7.15	-7.61	0.92	0.46
Allowable deflections	-7.5	-7.5			
Is the draft larger than the limits of 2.5m?	Yes	Yes			



(a) Without gill cells

(b) With gill cells

Fig. 4.6 Deflection surfaces of the floating container terminal with and without gill cells



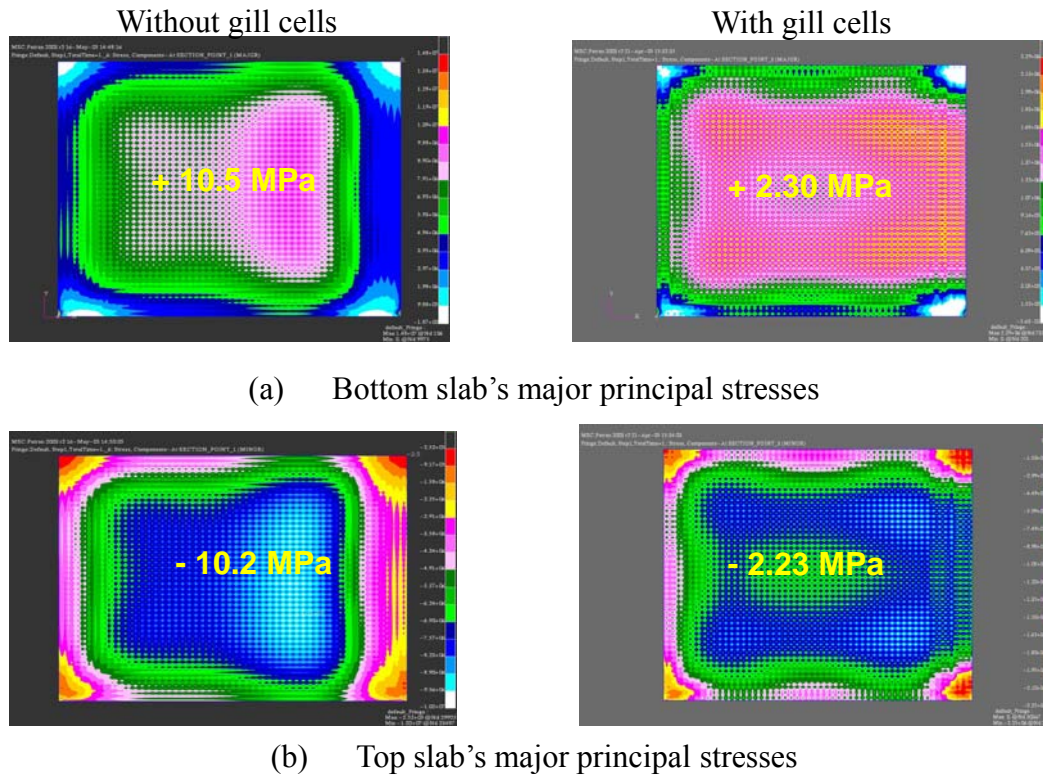


*Fig. 4.7 Stress contours of the floating container terminal with and without gill cells*

The positions of gill cells affect the differential deflection. So it is important to determine where the gill cells should be placed. In the following chapter, the procedure of the optimization exercise by implementing the genetic algorithm and interfacing genetic algorithm with finite element software ABAQUS to determine the optimal layouts of gill cells will be presented.

## **OPTIMAL LAYOUTS OF GILL CELLS**

In Chapter 4, we have concluded that the controlling design criterion for the floating container terminal is the between-rail gradient of the quay canes. In order to satisfy the tight tolerance of the between-rail gradient, we have proposed the innovative concept of gill cells. In this chapter, we shall examine sensitivity and the optimal layout of gill cells for reducing the differential deflection of floating structures under non-uniform loads. For the optimization exercise, we develop a computer code that makes use of genetic algorithms and an interface program that links the genetic algorithms code to ABAQUS that performs the finite element analysis. As an illustration of the optimization technique, we solve some examples involving square and rectangular floating structures. The optimal layout solution will be measured against various layouts of gill cells to assess the sensitivity of the gill cell positions in reducing the differential deflection of floating structures.

### **5.1 Proposed Location Patterns of Gill Cells**

#### **5.1.1 Problem Definition**

Consider a floating concrete structure of 200m x 180m x 5m comprising of compartments with dimensions 5m x 5m x 5m. The walls have a thickness of 300mm and the top and bottom floor slabs have a thickness of 500mm. Its central portion covering an area of 140m x 120m carries a heavy load 50kN/m<sup>2</sup> as shown in Fig. 5.1.

Assuming that the floating structure is held in place by the station keeping system, the load causes the floating structure to deform in a dish-like shape. The central deflection and the corner deflection lead to a large differential deflection and the problem at hand is to reduce this differential deflection by using a prescribed number of gill cells.

For the considered example problem, we assume that the floating structure is made from concrete with density of  $1900\text{kg/m}^3$ , Young's modulus of 22.9 GPa and Poisson's ratio of 0.2. Owing to symmetry of the floating structure and loading, we only need to consider a quadrant of the structure model having dimensions 100m x 90m x 5m with the implementation of appropriate boundary conditions at the lines of symmetry. At the axis line in the X direction (see Fig. 5.2), the degrees of freedom of the structure are constrained to only the X and Z directions whilst at the axis line in the Y direction, the degrees of freedoms of the structure are constrained to only the Y and Z directions. In using the finite element software ABAQUS for determining the deflection of the floating structure, we adopt the 4-node, thin-plate elements (QUAD type: S4R5) for the top slab, bottom slab and vertical walls. Elastic Winkler springs are adopted to simulate the buoyancy force of the sea-water. At the gill cells, the Winkler springs are removed as there are no buoyancy forces. The model of one quarter of the structure is shown in Fig. 5.2.

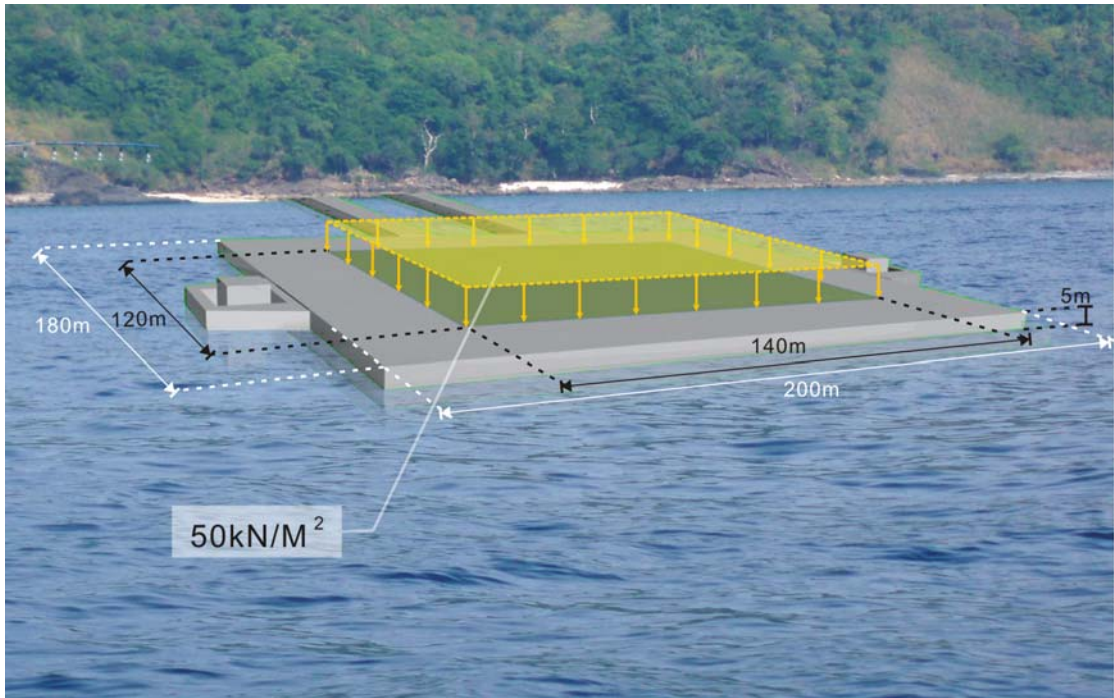


Fig. 5.1 Floating structure carrying heavy loads in the central portion

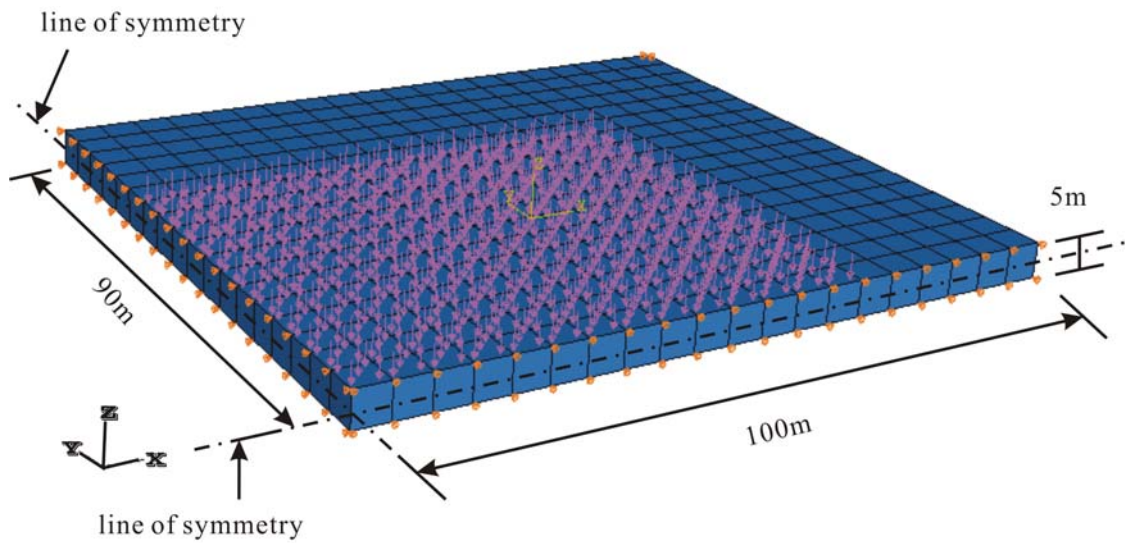


Fig. 5.2 Loading and boundary condition of a quarter of the structure

### 5.1.2 Proposed Patterns and Results

In this section, we will propose several patterns of gill cells layouts to see their effect on reducing the differential deflection. Figures 5.3 (a) to 5.3 (f) show the L-shape pattern at locations, black areas represent the normal cells whereas the white areas represent the gill cells.

In all these patterns, the gill cells are assumed to take up 20% of the total compartments of the floating structure. Table 5.1 shows the deflection results for the respective gill cell layout design. The gradient that equals to differential deflection divided by half length of the floating structure is also determined.

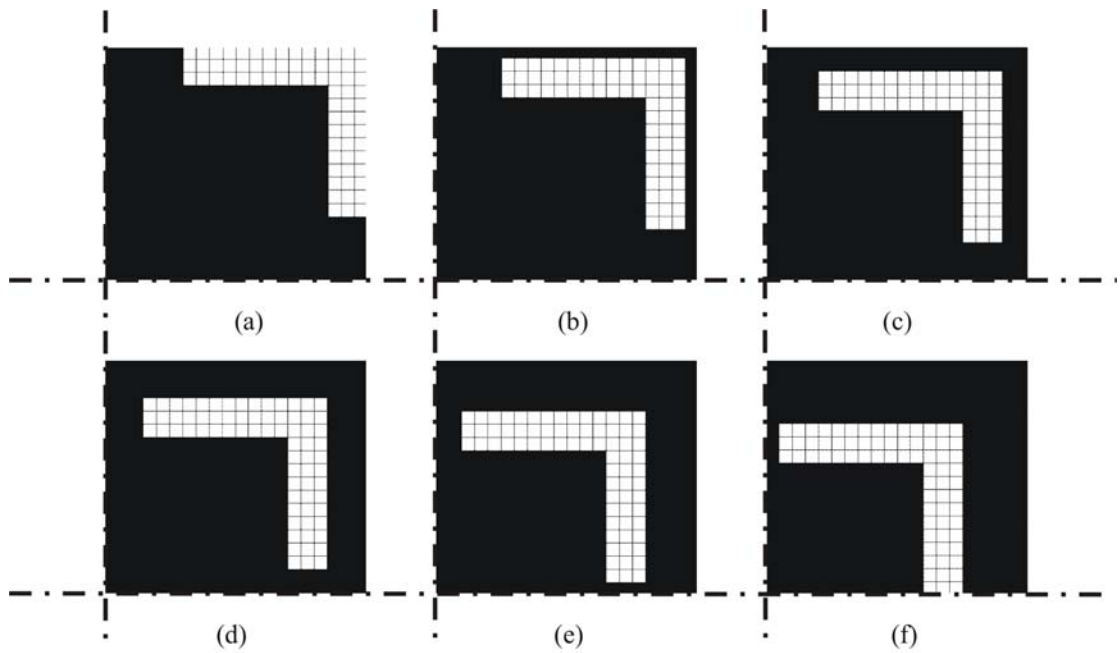
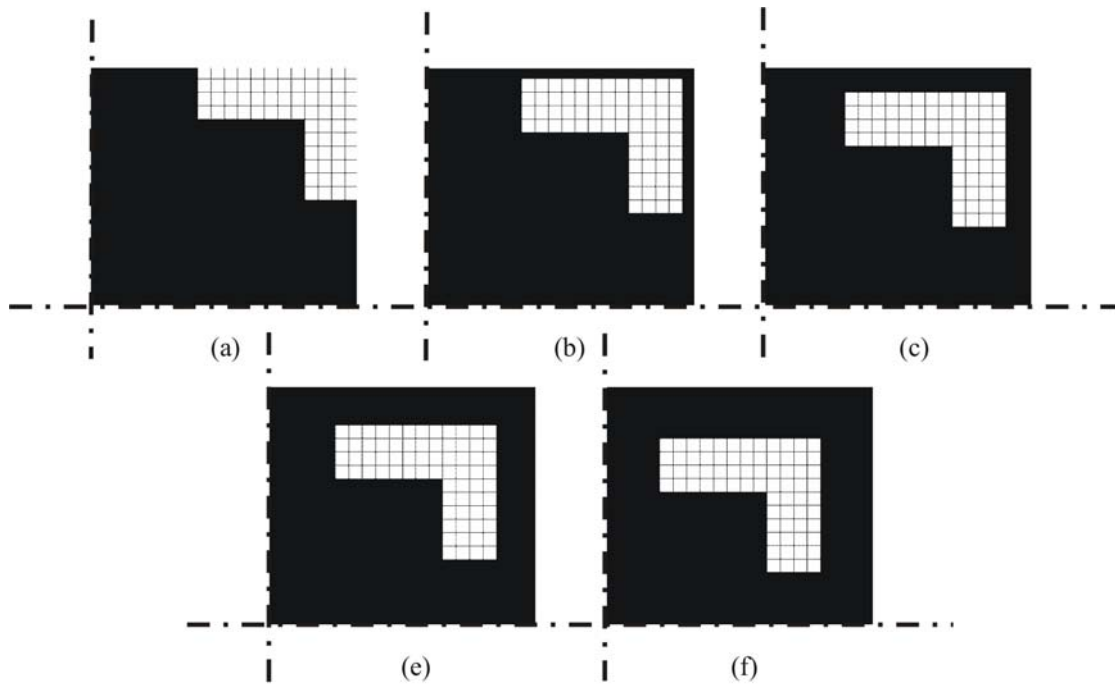


Fig. 5.3 Pattern 1 of gill cells' location ((a) to (f) represent the six types of layouts)

Table 5.1 Corresponding differential deflection and gradients associated to gill cells layout 1

Cases	Deflection in the center	Deflection in the corner	Differential deflection	Gradient (%)
Pattern 1	<b>20% gill cells in the structure</b>			
(a)	-3.158	-2.545	0.613	0.613
(b)	-3.189	-2.487	0.702	0.702
(c)	-3.224	-2.438	0.786	0.786
(d)	-3.263	-2.396	0.867	0.867
(e)	-3.306	-2.361	0.945	0.945
(f)	-3.353	-2.33	1.023	1.023

Figure 5.4 shows the second proposed pattern of location of 20% gill cells in the structure in which the gill cells are similar to pattern 1 but they are placed closer to the corners. Table 5.2 shows the corresponding results for this second pattern layout of gill cells.



*Fig. 5.4 Pattern 2 of gill cells' location  
((a) to (e) represent the five types respectively)*

*Table 5.2 Corresponding differential deflection and gradients associated to gill cells layout 2*

Cases	Deflection in the center	Deflection in the corner	Differential deflection	Gradient (%)
Pattern 2	<b>20% gill cells in the structure</b>			
(a)	-3.156	-2.564	0.592	0.592
(b)	-3.186	-2.502	0.684	0.684
(c)	-3.222	-2.449	0.773	0.773
(d)	-3.262	-2.404	0.858	0.858
(e)	-3.306	-2.366	0.94	0.94

Figure 5.5 shows the third pattern of the locations of 20% of gill cells in which the gill cells are distributed in a square shape close to the corners. Figure 5.6 shows two other proposed patterns (pattern 4 and pattern 5) with 20% gill cells. These two patterns have the gill cells distributed at the edge areas. Table 5.3 shows the results of pattern 3, pattern 4 and pattern 5.

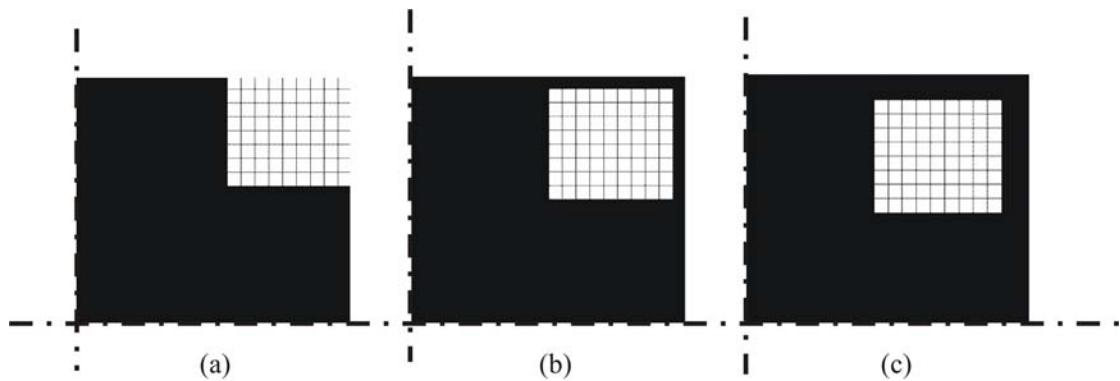


*Fig. 5.5 Pattern 3 of gill cells' location ((a) to (c) represent the three types respectively)*

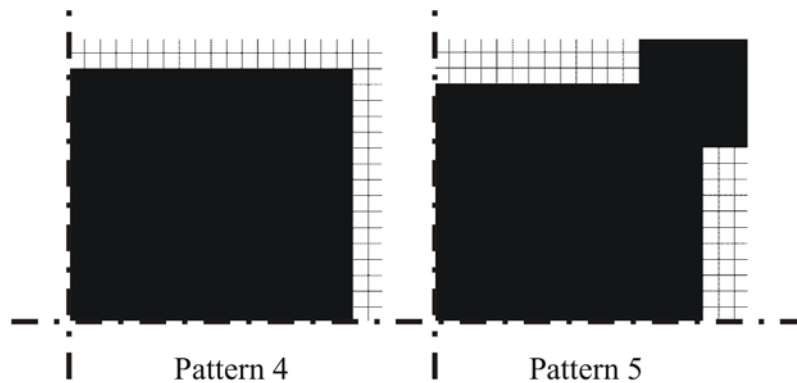


*Fig. 5.6 Patterns 4 and 5 of gill cells' location*

*Table 5.3 Corresponding differential deflection and gradients associated to gill cells layouts 3, 4, 5*

Cases	Deflection in the center	Deflection in the corner	Differential deflection	Gradient (%)
Pattern 3	<b>20% gill cells in the structure</b>			
(a)	-3.162	-2.566	0.596	0.596
(b)	-3.194	-2.502	0.692	0.692
(c)	-3.231	-2.449	0.782	0.782
Pattern 4	-3.175	-2.493	0.682	0.682
Pattern 5	-3.228	-2.402	0.826	0.826

From the corresponding results of the proposed patterns of gill cells' layouts, it can be seen that the closer these gill cells approach the corners and edges, the more effective they turn out to be. Though the perimeter layouts (see Fig. 5.3 (a) and Fig. 5.4 (a)) of gill cells perform quite satisfactory, we still do not know the best layout of gill cells. In the following sections, we will seek the optimal layout of gill cells that minimize the differential deflection by using Genetic Algorithms.

## 5.2 Optimization of the Gill Cells' Locations using Genetic Algorithms

### 5.2.1 Brief Introduction to Genetic Algorithms

#### 5.2.1.1 Concept of Genetic Algorithm

Genetic algorithm is a search technique used in computing to find true or approximate solutions to optimization and search problems (Simon and Sear, 1999). Genetic algorithms (GAs) are categorized as global search heuristics and they are a particular class of evolutionary algorithms that use techniques inspired by evolutionary biology such as inheritance, mutation, selection, and crossover.

The GA procedure is based on the Darwinian principle of survival of the fittest. An initial population is created containing a predefined number of individuals (or solutions), each of which is represented by a genetic string (incorporating the variable information). Each individual has an associated fitness measure, typically representing an objective value. The concept that fitter (or better) individuals in a population will produce fitter offspring is then implemented in order to reproduce the next generation. Selected individuals are chosen for reproduction (or crossover) at each generation,



with an appropriate mutation factor to randomly modify the genes of an individual, in order to develop the new population. The result is another set of individuals based on the original subjects leading to subsequent populations with better individual fitness. Therefore, the algorithm identifies the individuals with the optimizing fitness values, and those with lower fitness will naturally get discarded from the population. The GA procedure is illustrated in Fig. 5.7.

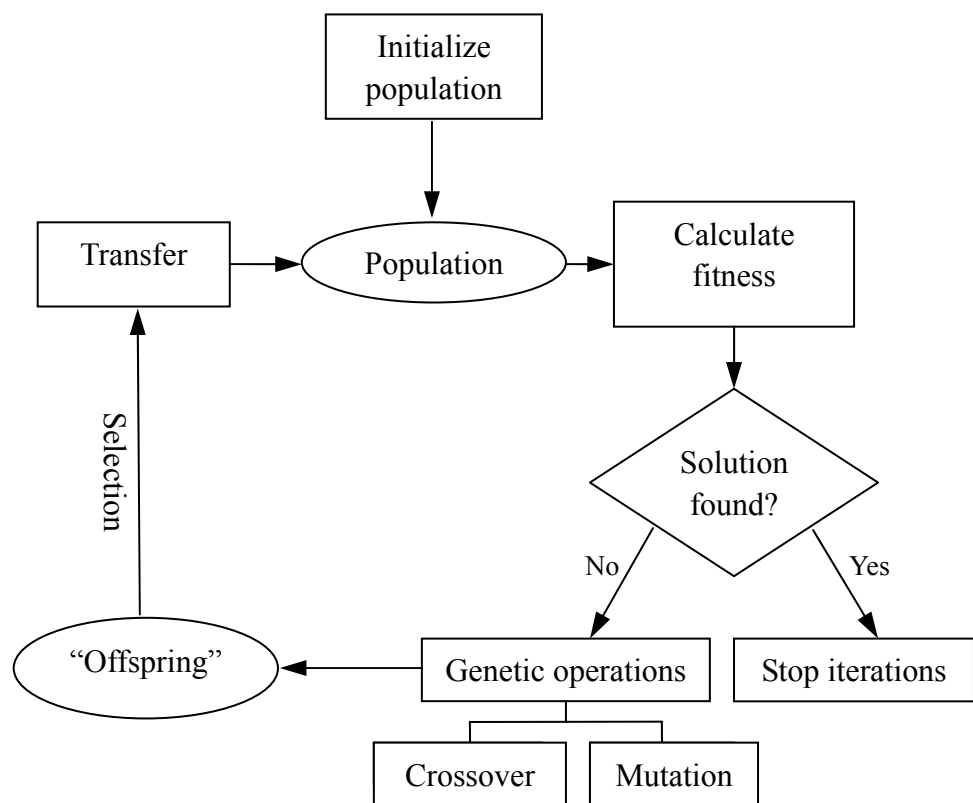


*Fig. 5.7 Flow chart of the basic steps in genetic algorithm*

### 5.2.1.2 Advantages of Genetic Algorithms

Evolutionary algorithms have been around since the early 1960s. They apply the rules of nature, i.e. the individuals, each of which represents a solution to a mathematical problem, survive through the selection. Genetic algorithms are so far

generally the best and most robust kind of evolutionary algorithms.

A GA has a number of advantages. It can quickly scan a vast solution set. Bad proposals do not affect the end solution negatively as they are simply discarded. The inductive nature of the GA means that it does not have to know any rules of the problem as it works by its own internal rules. This is very useful for complex or loosely defined problems. In a word, the major advantage of GA is their flexibility and robustness as a global search method.

### **5.2.2 GA Model of the Problem**

In this section, we will simulate our optimization of gill cells' layouts as a matter of evolution to implement the genetic algorithm. At the beginning, we have to make an assumption that each generation in GA has 100 individuals. In other words, the population size of the problem is 100.

The basic idea in implementing GA for the optimization exercise is to represent the compartments as a binary matrix (Wang and Tai, 2005). In this binary matrix, '0' represents the gill cell, which means that there is no buoyancy force under the compartment and '1' represents the normal cell, which means that there is a buoyancy force under the compartment. The advantage of doing so is that, in GA, binary list is the simplest form for reproduction (crossover and mutation). For each individual of the first generation in GA, a matrix with elements coinciding with the compartment numbers of the structure is produced and in this matrix '0's and '1's are randomly distributed to represent the gill cells and normal cells. For example, the model has 20 x 18 compartments and thus, in GA, we produce a 20 x 18 binary matrix as a genetic

string to represent an individual. Similarly, we produce 100 such matrices to make up the first generation of the population.

The next step after the initialization of the first generation is to calculate the differential deflection. This part will be discussed in the next section. For 100 individuals (binary matrices to be specific) of the first generation, we will obtain 100 results (i.e. 100 differential deflection values between the deflection of the central portion of the structure and the deflection at the edge). We next evaluate their fitness defined by the reciprocal value of the differential deflection  $\Delta$  and select “parents” (i.e. the binary matrices selected according to their fitness) for the next generation’s reproduction. For the selection mechanism, we adopt the Roulette Wheel Selection, also called the Monte Carlo Selection Algorithm. This algorithm seeks the “parents” according to their fitness criterion. The better the chromosomes are, the greater chances that they would be selected. The selected “parents” are then paired for reproduction (crossover and mutation) until the next generation of 100 individuals is formed. In the procedure of reproduction, two-point crossover method is adopted and the crossover rate is 0.7, while for the mutation rate, 0.01 is assumed. This completes one loop. In each loop, we have to check one pre-defined termination condition. If the termination condition is reached, the program will be stopped, otherwise it will keep on running. For our current problem, the results fluctuate about the mean values in the process of converging. So the termination of the program was performed manually when the observed differential deflection has reached a minimum value. For more information of the Monte Carlo Selection Algorithm and procedure of reproduction,

please refer to Appendix A.

### **5.2.3 Application Programming Interface (API) of ABAQUS**

In this section and section 5.2.4, we explain how the gill cells positions are adjusted to reduce the differential deflection calculated through developed interfacing program that links GA with the application programming interface (API) of ABAQUS. ABAQUS provides a scripting interface, which is an application programming interface to the model and data used by ABAQUS. The ABAQUS scripting interface is an extension of the Python object-oriented programming language. ABAQUS scripting interface scripts are Python scripts. With API, we can create and modify the components of an ABAQUS model, such as parts and loads, as well as read some results from the ABAQUS output database of an analysis. In other words, we can write command in the object-oriented programming language Python to execute all the procedures from pre-processing, such as creating models to post-processing, such as reading certain results from the output database.

ABAQUS provides a convenient way to retrieve the code of command used for modeling. We can first create the model in the pre-processing environment CAE, and then submit the job for analyses. In the mean time, ABAQUS will write all the commands that one has executed in CAE to a RPY file in Python. Thus, what one needs to do is to get the codes, modify them and put the GA code in the script (Lee and Kim, 2005).

#### 5.2.4 GA Interfacing with API of ABAQUS

Recall that the objective is to determine the differential deflection using ABAQUS for each individual of every generation according to the individual's genetic string (the binary matrix to be specific) and to evaluate the fitness of this differential deflection in GA. Then we need to integrate the code of GA with the code of procedure command in ABAQUS. Because each individual has a specific genetic string, which identifies its result, the idea is to define a function and make the specific genetic string as the argument of the function. The return value of this function will be the differential deflection calculated through ABAQUS. Thus, this function will form the part of evaluation in GA.

In the static analysis, the buoyancy force is simulated through the elastic Winkler springs and as mentioned before, the genetic strings are binary matrices. When the element in the matrix is "1", we have to attach a Winkler spring under the cell to simulate the buoyancy force of sea water. When the element is "0", we do not need to do that. In ABAQUS, the Winkler springs are defined through an element list which contains all the element numbers. Thus, we have to establish a one-to-one correspondence between the genetic strings and the element list. This one-to-one correspondence will reflect the variations of genetic strings to element numbers and thereby recognize the function of the genetic string as an argument. Meanwhile, we need to modify the computer code in order to make the differential deflection a return value of the function. Figure 5.8 shows the interfacing procedure. For detailed information about the code, please refer to Appendix B.

### Binary Matrix

In the first generation, the binary matrix is randomly created and in the following generations, the binary matrix is the “offspring” of the selected parents.

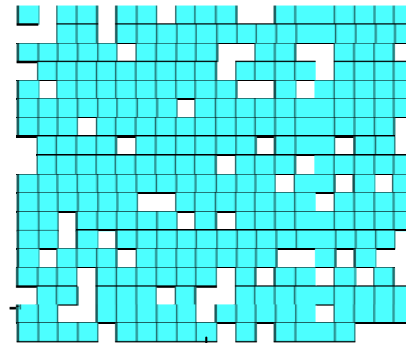
```
[[1, 0, 1, 1, 0, 1, 1, 0, 1, 1, 1, 0, 0, 1, 1, 1, 1, 1, 1, 1],  
[0, 0, 1, 1, 0, 1, 1, 1, 1, 1, 1, 1, 1, 1, 1, 1, 1, 1, 1, 1],  
[1, 1, 1, 1, 1, 0, 1, 1, 1, 1, 0, 0, 1, 1, 0, 0, 1, 1, 1, 0],  
[0, 1, 1, 1, 1, 1, 1, 1, 1, 1, 0, 1, 1, 1, 1, 0, 1, 1, 1, 1],  
[1, 0, 1, 1, 1, 1, 1, 1, 1, 1, 1, 0, 0, 1, 0, 1, 1, 1, 1, 1],  
[1, 1, 1, 1, 1, 1, 1, 1, 0, 1, 1, 1, 1, 1, 1, 1, 1, 1, 1, 1],  
[1, 1, 1, 0, 1, 1, 1, 1, 1, 1, 1, 1, 1, 1, 1, 1, 1, 1, 1, 0],  
[0, 1, 1, 1, 1, 0, 1, 1, 1, 1, 1, 1, 0, 1, 1, 1, 0, 1, 1, 0],  
[0, 1, 1, 1, 1, 1, 1, 1, 1, 1, 0, 1, 1, 1, 0, 1, 1, 1, 1, 1],  
[1, 1, 1, 1, 1, 1, 1, 1, 1, 1, 1, 1, 1, 0, 1, 1, 0, 1, 0, 1],  
[1, 1, 1, 1, 1, 0, 0, 1, 1, 1, 1, 1, 1, 1, 1, 0, 1, 1, 1, 1],  
[1, 1, 0, 1, 1, 1, 1, 1, 0, 1, 0, 1, 1, 1, 1, 1, 1, 1, 1, 1],  
[1, 1, 0, 1, 0, 1, 1, 1, 1, 1, 1, 1, 1, 1, 1, 1, 1, 1, 1, 0],  
[1, 0, 1, 1, 1, 0, 1, 1, 1, 1, 1, 1, 1, 0, 0, 1, 0, 1, 0, 0],  
[1, 1, 1, 0, 1, 1, 1, 1, 1, 1, 0, 1, 0, 1, 0, 1, 1, 0, 1, 0],  
[0, 1, 1, 0, 1, 1, 1, 0, 1, 0, 0, 1, 1, 1, 1, 1, 1, 1, 1, 1],  
[1, 1, 0, 0, 1, 1, 1, 1, 0, 1, 1, 1, 1, 1, 0, 1, 1, 1, 1, 1],  
[1, 1, 1, 1, 0, 1, 1, 1, 1, 1, 0, 1, 0, 1, 1, 1, 1, 0, 0, 0]]
```

### List of Element Numbers

Through the one-to-one correspondence, the binary matrix is transformed to the list of element numbers.

```
[361, 366, 370, 381, 388, 405, 415, 426, 465, 480, 496, 514, 532, 551, 533, 369, 374, 387,  
395, 404, 414, 425, 437, 450, 464, 479, 495, 513, 531, 550, 569, 552, 364, 368, 373, 379,  
386, 403, 413, 424, 436, 478, 494, 549, 568, 586, 372, 378, 385, 393, 402, 412, 423, 435,  
448, 477, 493, 511, 529, 567, 585, 602, 587, 371, 384, 392, 401, 411, 422, 434, 447, 461,  
476, 528, 566, 584, 601, 617, 603, 376, 383, 391, 400, 410, 421, 433, 446, 475, 491, 509,  
527, 546, 565, 583, 600, 616, 631, 618, 382, 390, 399, 420, 432, 445, 459, 474, 490, 508,  
526, 545, 564, 582, 599, 615, 630, 644, 398, 408, 419, 431, 458, 473, 489, 507, 525, 544,  
581, 598, 614, 643, 656, 407, 418, 430, 443, 457, 472, 488, 506, 524, 562, 580, 597, 628,  
642, 655, 667, 657, 406, 417, 429, 442, 456, 471, 487, 505, 523, 542, 561, 579, 596, 627,  
641, 666, 668, 416, 428, 441, 455, 470, 486, 541, 560, 578, 595, 611, 626, 640, 665, 676,  
686, 678, 427, 440, 469, 485, 503, 521, 540, 577, 610, 625, 639, 652, 664, 675, 685, 694,  
687, 439, 453, 484, 520, 539, 558, 576, 593, 609, 624, 638, 651, 663, 674, 684, 693, 701,  
452, 483, 501, 519, 557, 575, 592, 608, 623, 637, 650, 683, 700, 466, 482, 500, 537, 556,  
574, 591, 607, 622, 649, 672, 682, 699, 712, 499, 517, 555, 573, 590, 621, 660, 671, 681,  
690, 698, 705, 711, 717, 713, 498, 516, 572, 589, 605, 620, 634, 659, 670, 680, 689, 697,  
710, 716, 720, 718, 497, 515, 534, 553, 588, 604, 619, 633, 646, 669, 688, 696, 703, 709]
```

Through the definition of elastic foundation in ABAQUS, the genetic string (binary matrix) of each individual was reflected to the ABAQUS. (White areas represent the gill cells)



The script will be sent to the solver of ABAQUS and the calculated results are shown.

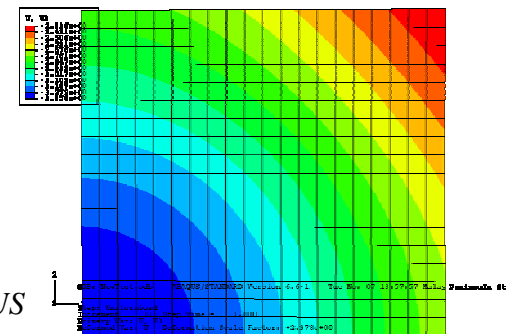
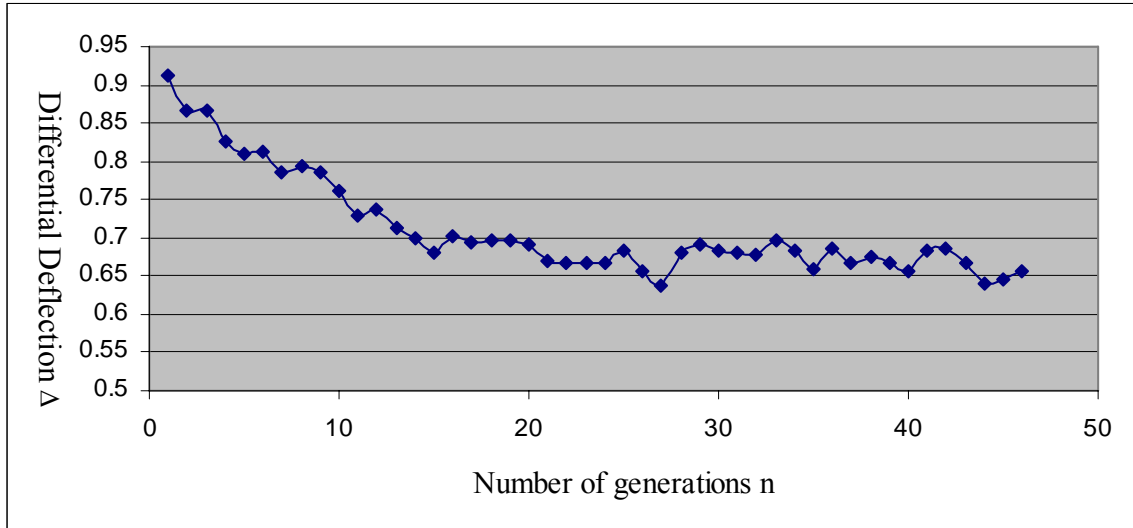


Fig. 5.8 Procedure of GA interfacing with ABAQUS

### **5.2.5 Results of Optimal Layouts**

Although we only consider a quarter of the structure, there are still 360 variables (compartments) in the binary matrix. In order to speed up the convergence, we begin by combining four variables into one variable and coarsely identify the location of gill cells and then we refine the layout based on the areas identified previously. We shall refer them as “coarse identification” and “refinement”.

The structure model of current problem has a plan dimension of 200m x 180m with each compartment of 5m by 5m. Thus, a quarter of the floating container terminal has 360 compartments and if we compact four compartments to one large compartment, we need to deal with only 90 variables. Based on the assumption that we employ 20% of the compartments as gill cells, then the number of gill cells is 18. In the genetic algorithm model of the problem, each generation has 100 individuals, thus 100 differential deflection results are obtained. What we are concerned about is the best of each generation. As a result, we select the individual with the minimum differential deflection to represent the fitness of this generation. Figure 5.9 shows the convergence of the differential deflection over 50 generations. Each point in the diagram represents the minimum differential deflection of that generation.



*Fig. 5.9 Convergence of differential deflection with respect to generations*

We can see from Fig. 5.9 that after about 20 generations, the minimum differential deflection does not decrease significantly. Instead, the results fluctuate around the mean value of approximately 0.65. It appears that the program reaches its limitation when the minimum differential deflection of the generations attains a particular value. Figure 5.10 shows the gill cells' layout of some typical generations over about 50 generations in the "coarse identification" model.



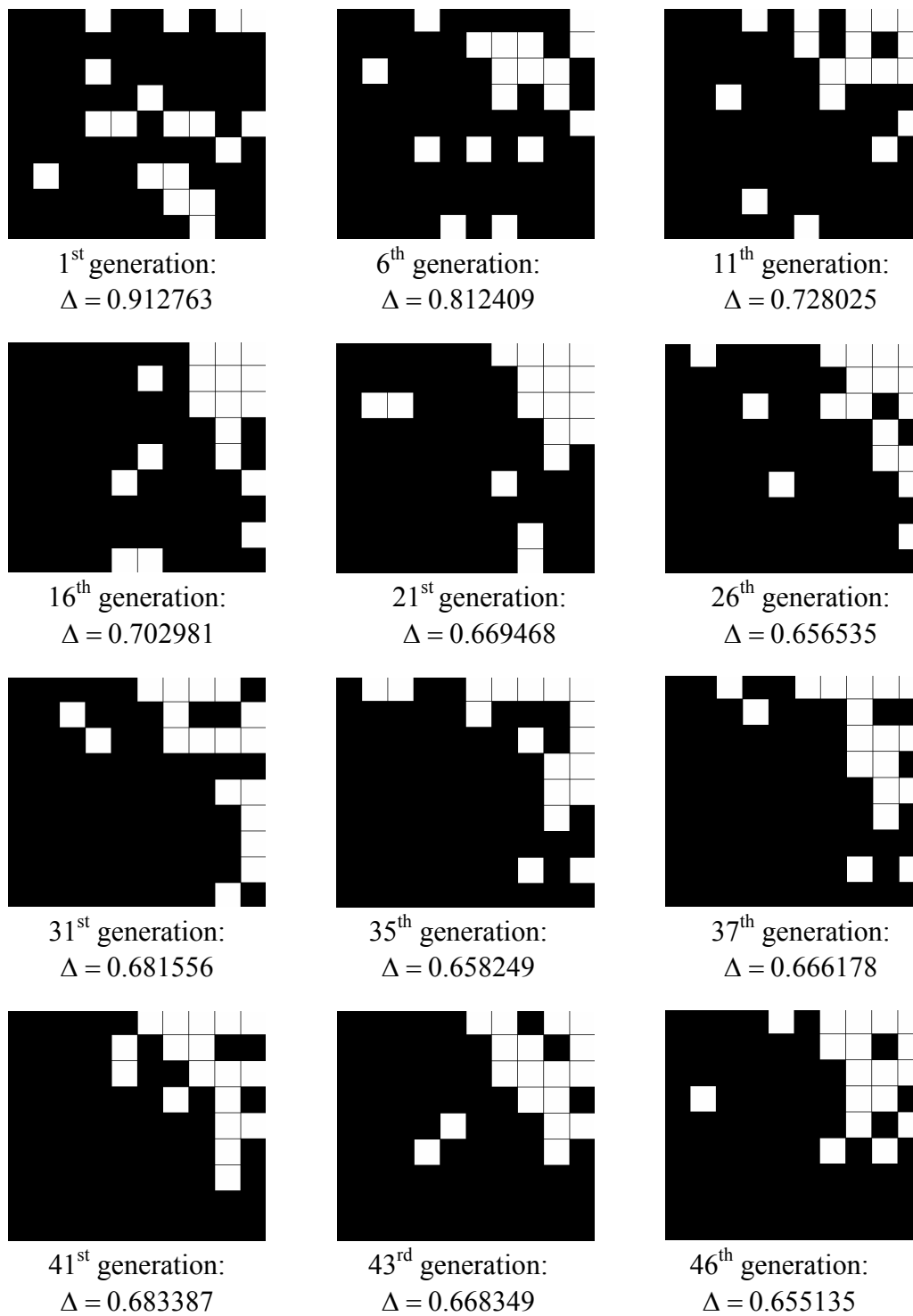


*Fig. 5.10 Layouts of the gill cells through “coarse identification” model*

Based on the gill cells' layout results throughout generations in the “coarse identification” model, we can conclude that, for those layouts yielding small differential deflections, the gill cells tend to merge at the corner areas in the white region as shown in Fig. 5.11.

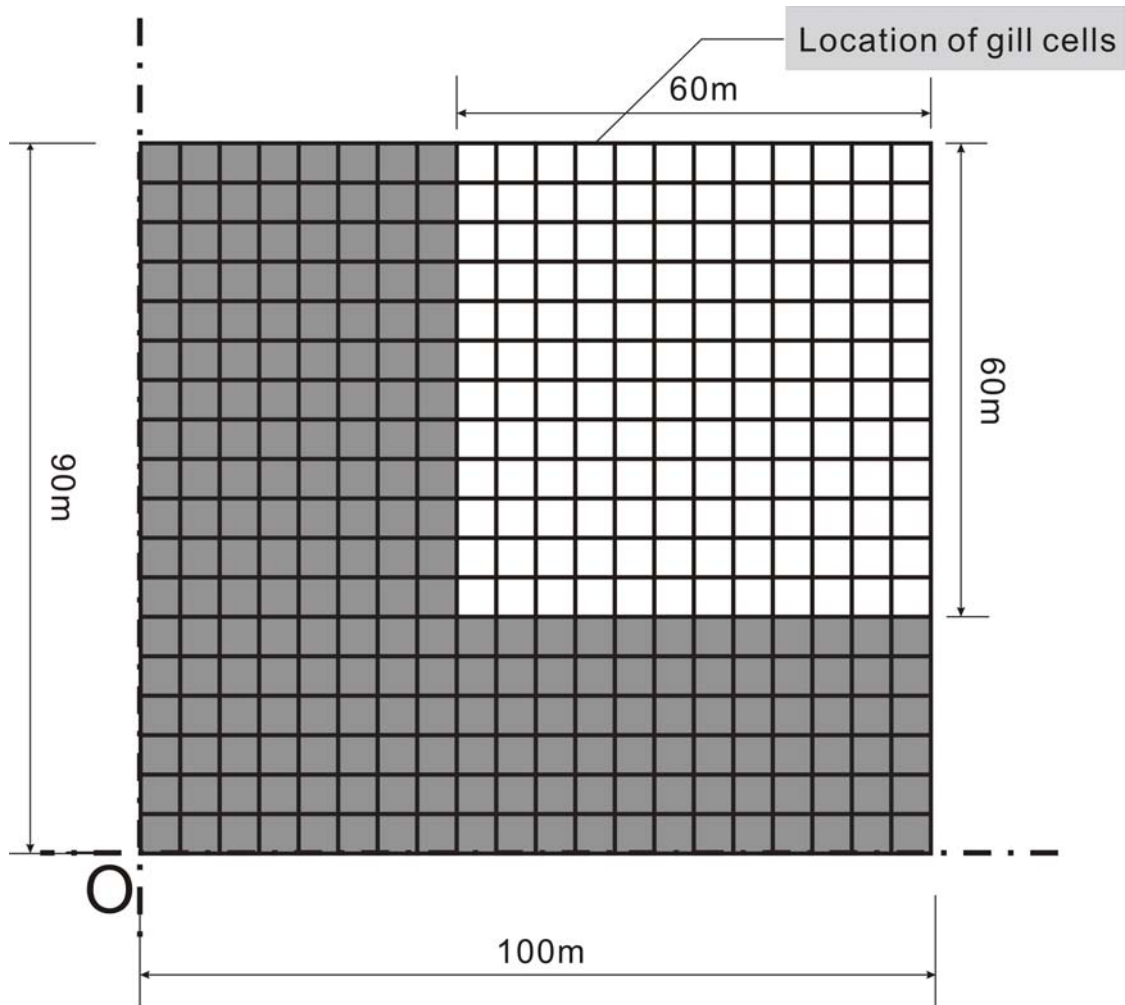


*Fig. 5.11 Quadrant of floating structure showing loaded area and location of gill cells*

Next we increase the number of gill cells from 90 to 144 and use the corner distribution (see Fig. 5.11) of gill cells as the initial design for further iterations in determining the optimal layout of the gill cells. To increase the sensitivity of the programming code, we also increase the load intensity to  $80\text{kN}/\text{m}^2$ . The decrease in the differential deflection for 80 generations is shown in Fig. 5.12. We can see from

the result that after 50 generations, the minimum differential deflections of generations begin to fluctuate around the mean value of 0.95 instead of decreasing further. After identifying the layout patterns, we switch the load intensity back to  $50\text{kN}/\text{m}^2$ . The patterns of the gill cell locations associated with various generations and the corresponding differential deflection values under  $50\text{kN}/\text{m}^2$  load intensity are shown in Fig. 5.13. The pattern for the gill cells location is examined and the optimal layout is decided from observing the trend of the movement of the gill cell locations in the optimization exercise. Based on judgment and from practical considerations, the optimal layout of the gill cells is decided. The optimal solution requires the gill cells to be distributed in a triangular shape close to the corners as shown in Fig. 5.14. By performing the analysis, the differential deflection value for this optimal layout is 0.566. Note that if the same number of gill cells is distributed along the four edges, the differential deflection value is 0.682 (see Pattern 4 of proposed layout of gill cells in Fig. 5.6 and Table 5.3). This means that the optimal layout of gill cells can significantly reduce the differential deflection, for this case by approximately 20%. Figure 5.15 shows a summary of the differential deflection obtained by using various patterns of gill cells layouts.

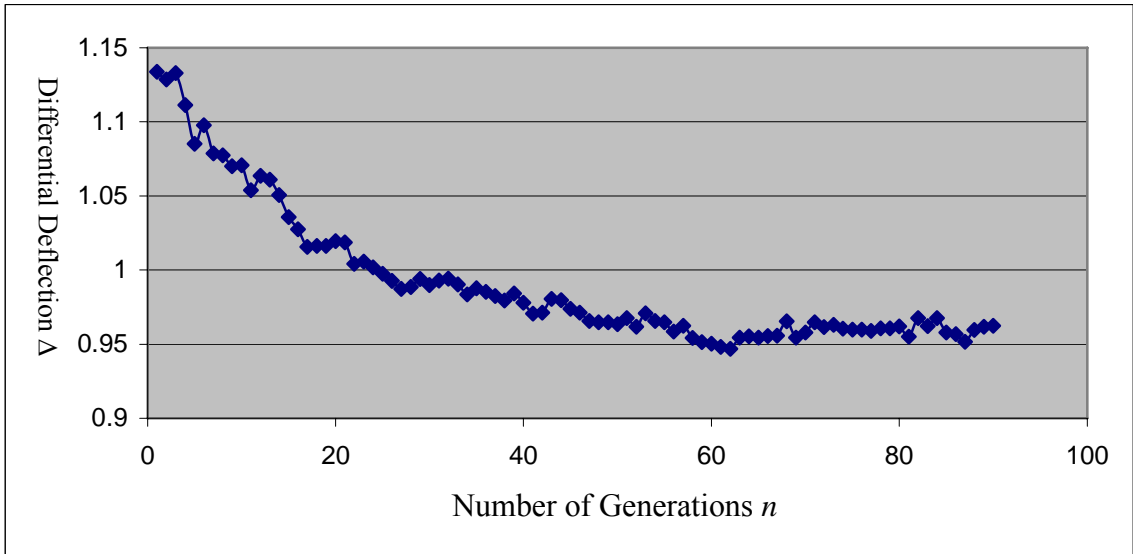
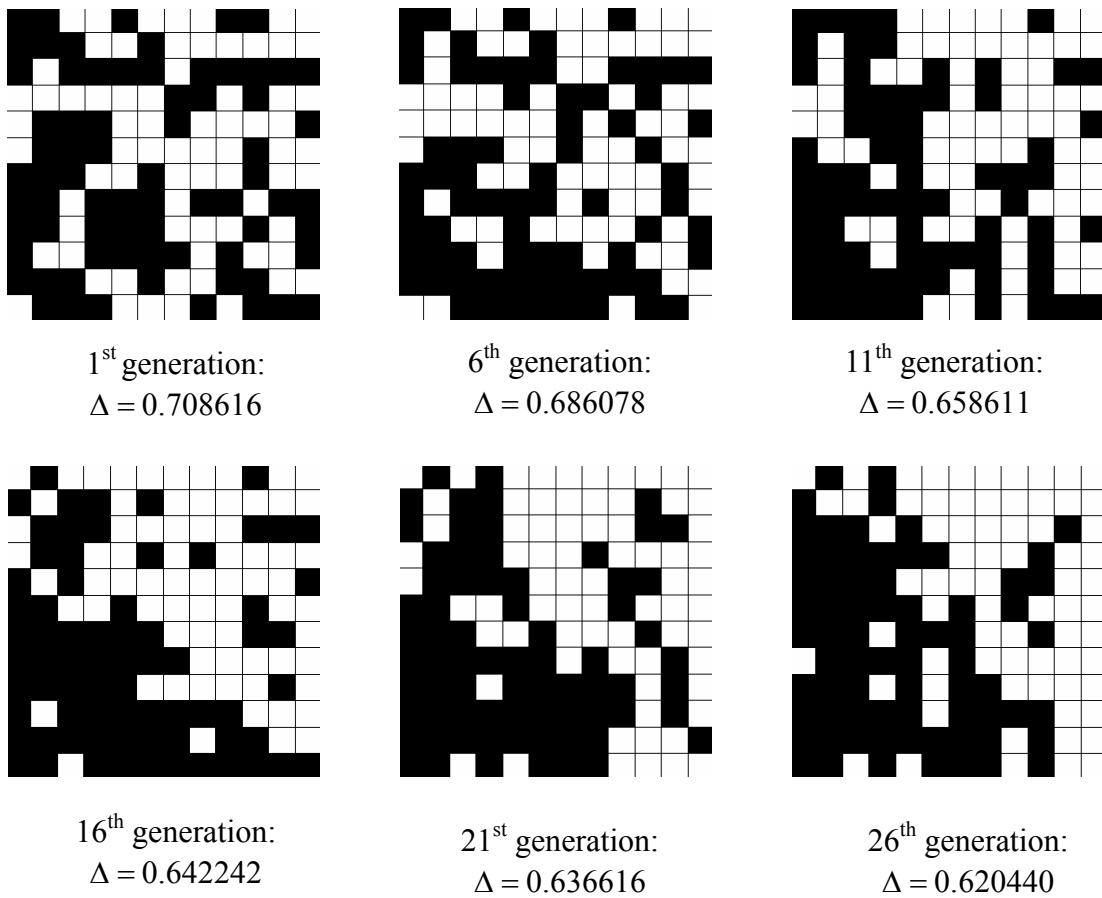
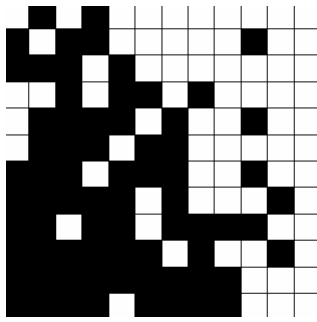
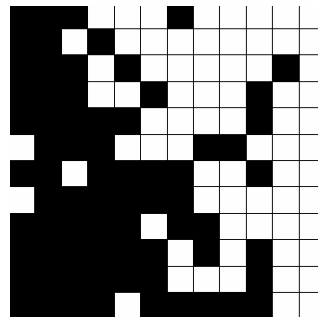


Fig. 5.12 Convergence of differential deflection with respect to number of generations

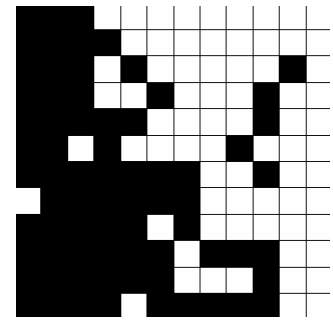




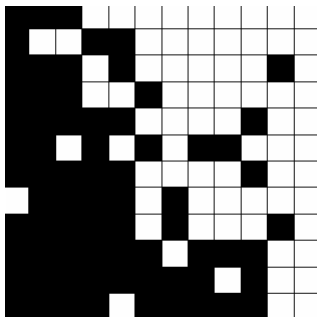
31<sup>st</sup> generation:  
 $\Delta = 0.620520$



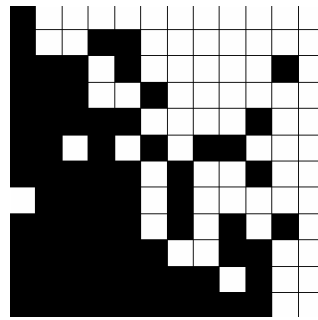
36<sup>th</sup> generation:  
 $\Delta = 0.615897$



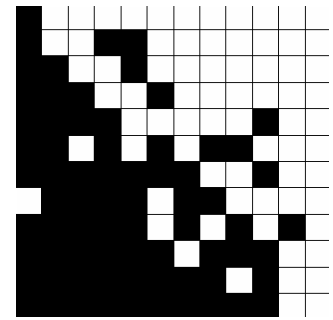
41<sup>st</sup> generation:  
 $\Delta = 0.606666$



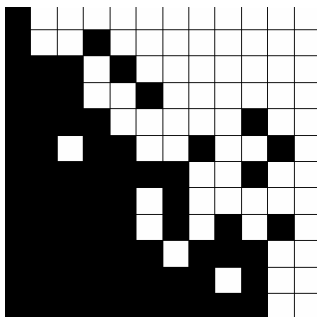
46<sup>th</sup> generation:  
 $\Delta = 0.607046$



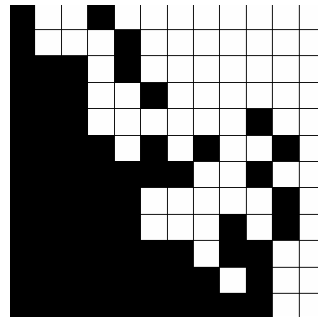
51<sup>st</sup> generation:  
 $\Delta = 0.604725$



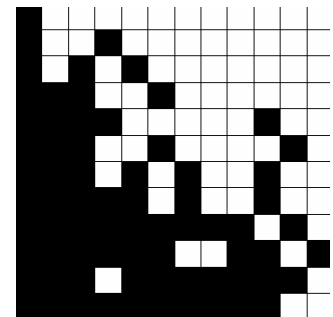
56<sup>th</sup> generation:  
 $\Delta = 0.599075$



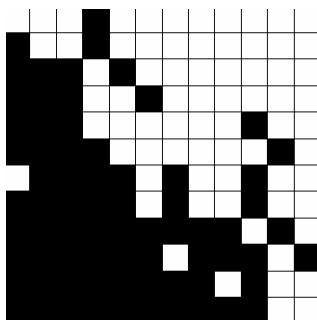
61<sup>st</sup> generation:  
 $\Delta = 0.592597$



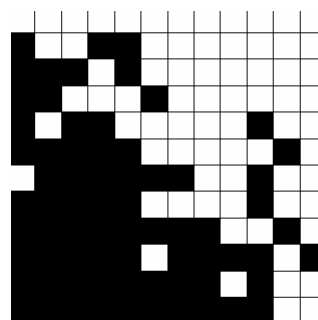
66<sup>th</sup> generation:  
 $\Delta = 0.597198$



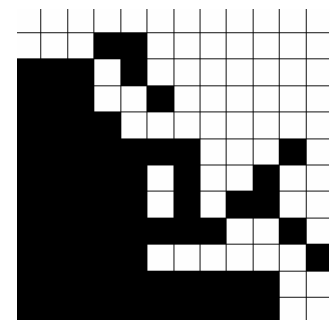
71<sup>st</sup> generation:  
 $\Delta = 0.603035$



76<sup>th</sup> generation:  
 $\Delta = 0.599913$

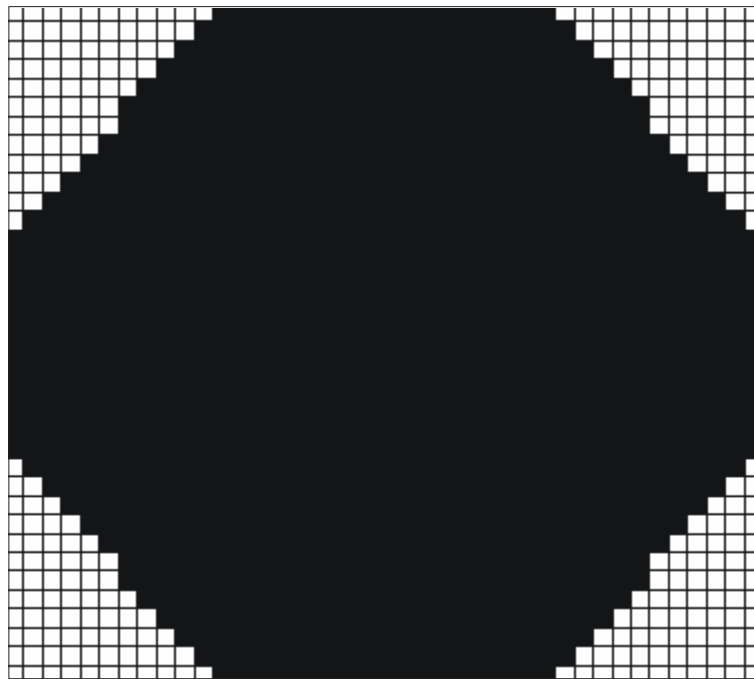


81<sup>st</sup> generation:  
 $\Delta = 0.596902$



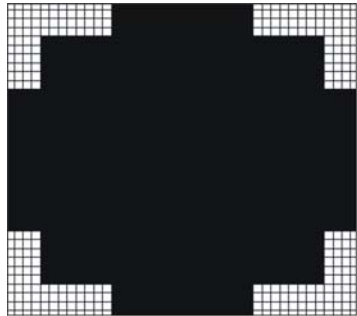
86<sup>th</sup> generation:  
 $\Delta = 0.594733$

*Fig. 5.13 Layouts of gill cells through “refinement” model*

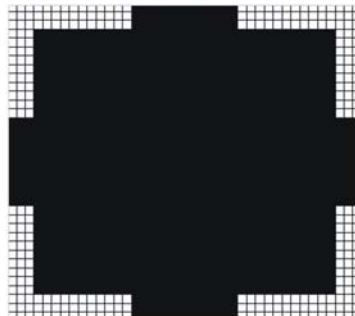


Differential Deflection  $\Delta = 0.566367$

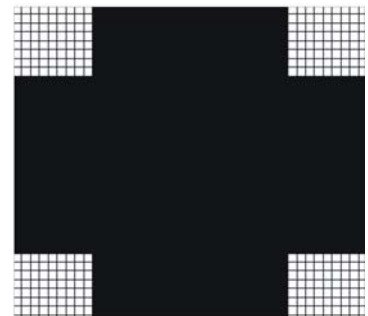
*Fig. 5.14 Optimal layout of gill cells with 20% gill cells*



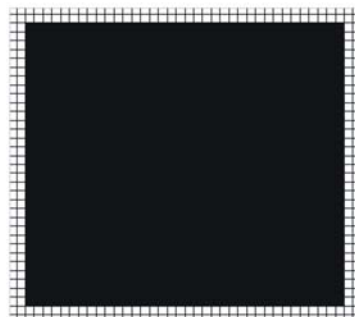
$\Delta = 0.592$



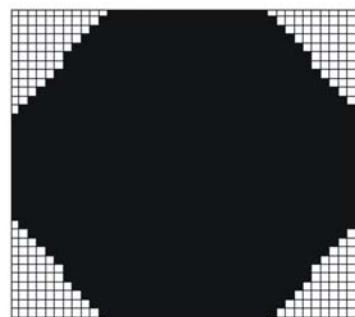
$\Delta = 0.613$



$\Delta = 0.596$



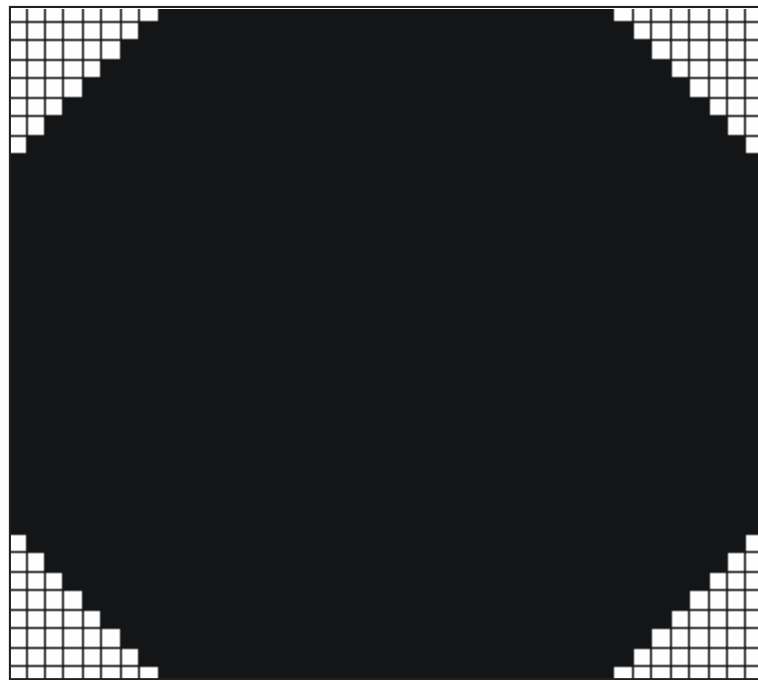
$\Delta = 0.682$



$\Delta_{optimal} = 0.566$

*Fig. 5.15 Comparison between various patterns of gill cells layouts*

If it is modeled in the shape of square, the layout of gill cells should also be symmetric according to the diagonal. Of course with a large percentage of gill cell, say, 20%, the freeboard of the floating structure decreases due to the loss of buoyancy. If a larger value of freeboard is needed, we need to decrease the percentage of gill cells. For example, in the above problem where 20% of the compartments are assigned to be gill cells, the free board is 2.418m and if one uses the same layout pattern but reduce the percentage of gill cells to 10% as shown in Fig. 5.16, the freeboard increases to 2.854m but the differential deflection increases to 0.767m.



Differential Deflection  $\Delta = 0.767$

*Fig. 5.16 Optimal layout of gill cells with 10% gill cells*

### 5.3 Layouts of Gill Cells for Different Loading Patterns and Shapes of VLFS

In the foregoing example of floating container terminal, the aspect ratio is close to unity, but there are many floating structures with large aspect ratios, such as the mega-float with an aspect ratio of  $L/B = 1000/60$ . The optimal layout of gill cells may turn out to be of other patterns for floating structure shapes. By performing the optimization exercise on a floating structure with an aspect ratio of four, loaded as shown in Fig. 5.17a and restricting the percentage of compartments to 20% for gill cells, it was found that the optimal layout of gill cells are such that they are distributed towards both end portions as shown in Fig. 5.17b.

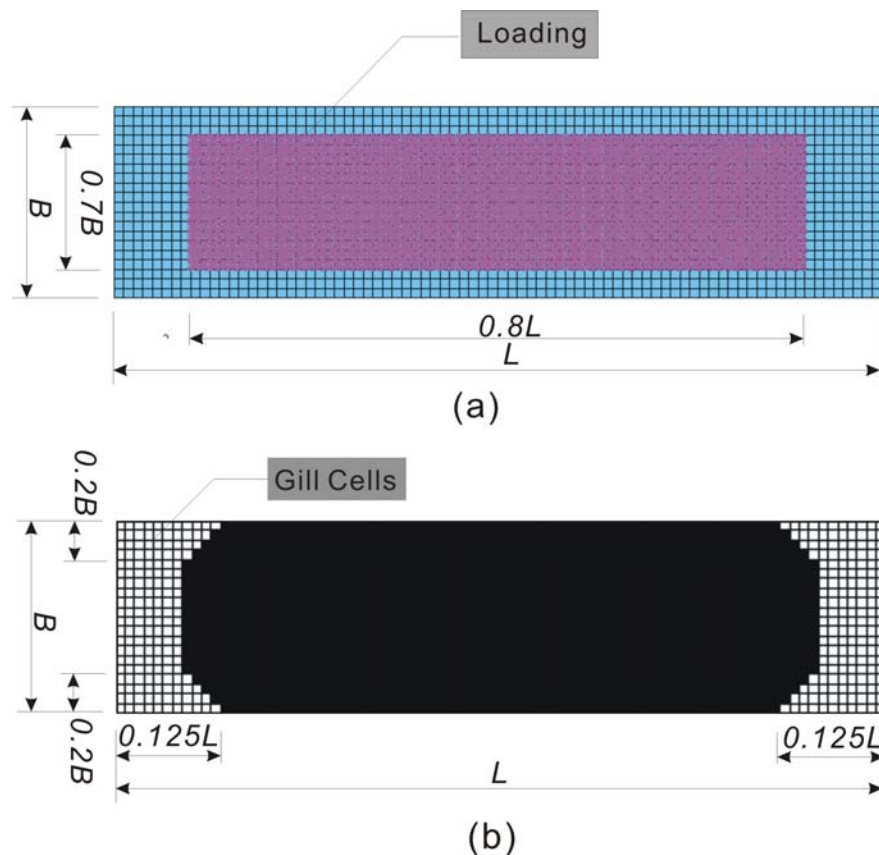


Fig. 5.17 (a) Loading area and (b) Optimal layout of gill cells for floating structure with  $L/B=4$



## **CONCLUSIONS AND RECOMMENDATIONS FOR FUTURE STUDIES**

### **6.1 Conclusions**

In this thesis, we first discussed the sea space utilization in the past few years and introduced the very large floating structure, a relatively new technology to create land from the sea. We then focus attention on VLFS as a very large floating container terminal. This focus is promoted by the need to build container terminal in large water depth so as to accommodate mega-container ships. There is a current trend of building such mega-container ships to increase transshipment capacity (Baird, 2002). A preliminary design of the floating container terminal made from high performance concrete is presented based on the functional and operational requirements given by PSA and MPA engineers. The container terminal is modeled and static analyses are performed for the structure under self-weight and live load due to container loadings. We also provide the detail design of a typical watertight compartment of the floating container terminal.

From the static analysis of the floating container terminal, it is found that the floating container terminal suffers from the problem of “dishing effect”. The large differential deflection between central portion and the edge areas of the container terminal due to the heavy container loads on the central stacking yard cause some

operational problems for the quay cranes. Note that the smooth operation of quay cranes must satisfy a tight tolerance value of 0.4 of the between-rail gradient of quay cranes.

In order to solve this large differential deflection problem, we introduce the innovative concept of “gill cells” and performed some analyses of the floating container terminal with gill cells. Gill cells are compartments in the floating structure where the bottom surface is perforated to allow water to flow freely in and out. At the locations of these gill cells, the buoyancy forces are eliminated. The gill cells, when placed appropriately, turn out to be very effective as the differential deflection of the floating container terminal is considerably reduced. For maximum reduction of the differential deflection, the optimal layout of gill cells is to be sought. In determining the optimal layouts of gill cells for a general floating structure, a computer code that makes use of the genetic algorithms and an interfacing code to link the genetic algorithms for optimization exercise with the finite element software ABAQUS for analyses are developed. The computers codes are demonstrated on an example problem in which the floating structure has an aspect ratio close to unity and is heavily loaded in the central portion. The optimal solution requires the gill cells to be distributed in a triangular shape close to the corners. The optimal solution was compared with various patterns of gill cells layouts (see Fig. 5.15) and it was shown that the optimal solution is more effective in reducing the differential deflection. It is thus important to determine the optimal layout of gill cells.

## 6.2 Recommendations for Future Research

There are several directions for the future research. We may consider improving the programming code which links genetic algorithms to the finite element software ABAQUS in the optimization exercise to increase the sensitivity of the convergence of the results.

We can also develop further the detail design of gill cells such as the number and dimension of the holes or slits of gill cells and so on. We may also consider the hydrodynamic effect of the sea water to the floating structures with gill cells when determining the differential deflection through ABAQUS as the sea state may not always be calm.

Further study should be made to try to expand the optimization technique on rectangular plates to floating structures with different shapes and under various loading configurations. This is because there is a need for other shapes and loadings of floating structures for different applications. By implementing the optimization technique, we may determine the optimal layouts of gill cells for more complex cases.

## REFERENCES

- Suzuki H. (2005). Overview of megafloat: Concept, design criteria, analysis, and design. *Marine Structures*, **18** (2), 111-132.
- Baird A.J. (2002). Container vessels in the new millennium: implications for seaports. *Ocean Yearbook*, **16**, 300-327.
- Wang C.M. and Wu T.Y. (2005). Research into super-large floating container terminal. *Research Report No. 1*, submitted to MPA and JCPL, Center for Offshore Research and Engineering, National University of Singapore: Singapore.
- Wang C.M., Yao Z.J. and Wee T.H. (2006). Research into super-large floating container terminal: Design of typical cell in floating structure, joining system and estimated cost. *Report No. 4*, submitted to MPA and JCPL, Center for Offshore Research and Engineering, National University of Singapore: Singapore.
- BS8110 (1985): A British Standard for the design and construction of reinforced and prestressed concrete structures. *BSI*, London.
- Young W.C. and Budynas R.G. (2002). *Roark's Formulas for Stress and Strain (7<sup>th</sup> Edition)*. McGraw-Hill, New York, NY.
- Wang C.M., Wu T.Y., Choo Y.S., Ang K.K., Toh A.C., Mao W.Y. and Hee A.M. (2006). Minimizing differential deflection in a pontoon-type, very large floating structure via gill cells. *Marine Structures*, **19** (1), 70-82.
- Simon M and Sear P. (1999). An overview of genetic algorithm for the solution of optimization problems, *Computers in Higher Education Economics Review*, **13** (1), 16-20.
- Wang S.Y. and Tai K. (2005). Structural topology design optimization using genetic algorithms with a bit-array representation. *Comput Method Appl. Mech. Engrg.* **194**, 3749-3770.
- Lee W. and Kim H.Y. (2005). Genetic Algorithm implementation in python. Computer and Information Science, Fourth Annual ACIS International Conference, Jeju island, South Korea.
- Fujikubo M. (2005). Structural analysis for the design of VLFS. *Marine Structure*, **18** (2), 201-226.
- Martin L.H. (1989). *Structure Design in Concrete to BS8110*. Edward Arnold, London.

Rozvany GIN. and Karihaloo BL. (1985). *Structural Optimization*. Kluwer Academic Publishers, Netherlands.

Guler K. and Celep Z. (1995). Static and dynamic responses of a circular plate on a tensionless elastic foundation. *Journal of Sound and Vibration*, **183** (2), 185-195.

Reddy J.N. (2006). *An Introduction to the Finite Element Method (3<sup>rd</sup> Edition)*. McGraw-Hill, New York, NY.

Bathe K.J. (1996). *Finite Element Procedures*. Prentice Hall, Upper Saddle River, New Jersey.

Timoshenko S. and Woinowsky-Krieger S. (1984). *Theory of Plates and Shells (2<sup>nd</sup> Edition)*. McGraw-Hill, Singapore.

Allen A.H. (1988). *Reinforced Concrete Design to BS8110: Simply Explained*. E. & F.N. Spon, London; New York.

ABAQUS/Standard User's Manual. Version 6.6. Hibbitt, Karlsson & Sorensen, Inc, USA. <http://www.abaqus.com>

ABAQUS/Scripting User's Manual. Version 6.6. Hibbitt, Karlsson & Sorensen, Inc, USA. <http://www.abaqus.com>

## **GENETIC ALGORITHMS**

### **Roulette Wheel Selection**

Selection is the stage of a genetic algorithm in which individual genomes are chosen from a population for later breeding (recombination or crossover). There are several genetic selection algorithms. The roulette wheel selection is one of the most common ones and can be implemented as follows:

1. The fitness function is evaluated for each individual, providing fitness values, which are then normalized. Normalization here means multiplying the fitness value of each individual by a fixed number, so that the sum of all fitness values equals unity.
2. The population is sorted by descending fitness values.
3. Accumulated normalized fitness values are computed (the accumulated fitness values of an individual is the sum of its own fitness value plus the fitness values of previous individuals). The accumulated fitness of the last individual should of course be unity (otherwise something has gone wrong in the normalization step).
4. A random number  $R$  between 0 and 1 is chosen.
5. The selected individual is the first one whose accumulated normalized value is greater than  $R$ .

## **Reproduction (Crossover and Mutation)**

### **Crossover**

In genetic algorithms, crossover is a genetic operator used to vary the programming of a chromosome or chromosomes from one generation to the next. It is an analogy to reproduction and biological crossover, upon which genetic algorithms are based. There are several ways of crossover: one point crossover, two points crossover, “cut and splice”, uniform crossover and half uniform crossover.

- **One Point Crossover:** A crossover point on the parent organism string is selected. All data beyond that point in the organism string is swapped between the two parent organisms. The resulting organisms are the children.
- **Two Point Crossover:** Two point crossover calls for two points to be selected on the parent organisms, rendering two child organisms.
- **“Cut and Splice”:** this approach results in a change in length of the children string. The reason for this difference is that each parent string has a separate choice of crossover point.
- **Uniform Crossover and Half Uniform Crossover:** In both these schemes, the two parents are combined to produce two new offsprings. In the uniform crossover scheme, individual bits in the string are compared between two parents. The bits are swapped with a fixed probability, typically 0.5. In the half uniform crossover, exactly half of the nonmatching bits are swapped. Thus first Hamming distance (the number of differing bits) is calculated. This number is divided by two. The resulting number is how many of the bits that do not

match between the parents will be swapped.

## **Mutation**

In genetic algorithms, mutation is a genetic operator used to maintain genetic diversity from one generation of a population of chromosomes to the next. It is analogous to biological mutation. The classical example of a mutation operator involves a probability that an arbitrary bit in a genetic sequence will be changed from its original state. A common method of implementing the mutation operator involves generating a random variable for each bit in a sequence. This random variable tells whether or not a particular bit will be modified.

The purpose of mutation in GAs is to allow the algorithm to avoid local minima by preventing the population of chromosomes from becoming too similar to each other, thus slowing or even stopping evolution. This reasoning also explains the fact that most GA systems avoid only taking the fittest of the population in generating the next but rather a random (or semi-random) selection with a weighting toward those that are fitter.



## COMPUTER CODE

In this appendix, the computer codes compiled in PYTHON used in the optimization procedure is provided. The computer codes include:

- Genetic functions: mutation and crossover
- Objective function: the part of linking genetic algorithm with application programming interface of ABAQUS
- Execution of the first generation: the template of the evolution procedure throughout generations in genetic algorithm

### Genetic Function

```
# Make the elements in the array to crossover at crossover_rate
def bit_crossover(listA,listB):
    c = random.randint(0,(len(listA)-1))
    d = random.randint(0,(len(listA)-1))
    if c < d:
        pt1 = c
        pt2 = d
    else:
        pt1 = d
        pt2 = c
    if random.random() <= crossover_rate:
        tempA = listA[:pt1] + listB[pt1:pt2] + listA[pt2:]
        tempB = listB[:pt1] + listA[pt1:pt2] + listB[pt2:]
        listA = tempA
        listB = tempB
    return listA, listB

# Make the array to crossover
def chromosome_crossover(arrayA,arrayB):
    for i in range(len(arrayA)):
        arrayA[i],arrayB[i] = bit_crossover(arrayA[i],arrayB[i])
```

```

def mutate(arrayC):
    for i in range(len(arrayC)):
        if arrayC[i].__contains__(0) and arrayC[i].__contains__(1):
            m = random.randrange(len(arrayC[i]))
            n = random.randrange(len(arrayC[i]))
            while arrayC[i][m] == arrayC[i][n]:
                m = random.randrange(len(arrayC[i]))
                n = random.randrange(len(arrayC[i]))
            if random.random() <= mutation_rate:
                arrayC[i][m],arrayC[i][n] = arrayC[i][n],arrayC[i][m]
        else:
            pass
    return arrayC

```

## Objective Function

```

def getdeltaDisp(zijian):
    from abaqus import *
    from abaqusConstants import *
    session.Viewport(name='Viewport: 1', origin=(0.0, 0.0), width=159.375,
        height=153.4375)
    session.viewports['Viewport: 1'].makeCurrent()
    session.viewports['Viewport: 1'].maximize()
    from caeModules import *
    from driverUtils import executeOnCaeStartup
    import operator
    executeOnCaeStartup()
    openMdb(pathName='/proj4/pg/p50514r/Floating Plate.cae')
    #: The model database "/proj4/pg/p50514r/Floating Plate.cae" has been opened.
    session.viewports['Viewport: 1'].setValues(displayedObject=None)
    p = mdb.models['Floating Plate'].parts['Longwalls']
    session.viewports['Viewport: 1'].setValues(displayedObject=p)
    a = mdb.models['Floating Plate'].rootAssembly
    session.viewports['Viewport: 1'].setValues(displayedObject=a)
    session.viewports['Viewport: 1'].assemblyDisplay.setValues(interactions=ON,
        constraints=ON, connectors=ON, engineeringFeatures=ON)
    srf1 = mdb.models['Floating Plate'].rootAssembly-surfaces['BottomSurface']
    leaf = dgm.LeafFromMeshSurfaceSets(surfaceSets=(srf1, ))
    session.viewports['Viewport: 1'].assemblyDisplay.displayGroup.replace(
        leaf=leaf)
    session.viewports['Viewport: 1'].view.setValues(session.views['Front'])
    a = mdb.models['Floating Plate'].rootAssembly

```

```

s1 = a.instances['Whole-1'].faces
side2Faces1 = reduce(operator.add,[s1[i-1:i] for i in zijian])
a.Surface(side2Faces=side2Faces1, name='BottomSurface')
#: The surface 'BottomSurface' has been edited (288 faces).
session.viewports['Viewport: 1'].assemblyDisplay.setValues(interactions=OFF,
    constraints=OFF, connectors=OFF, engineeringFeatures=OFF)
mdb.jobs['NewTest'].submit(consistencyChecking=OFF)
mdb.jobs['NewTest'].waitForCompletion()
import odbAccess
odb = odbAccess.openOdb(path='NewTest.odb')
myAssembly = odb.rootAssembly
lastFrame = odb.steps['UniformLoad'].frames[-1]
displacement = lastFrame.fieldOutputs['U']
fieldValues = displacement.values
cornerNode = fieldValues[611].data[2]
centerNode = fieldValues[570].data[2]
deltaDisp = cornerNode-centerNode
odb.close()
return deltaDisp

```

## Execution of the First Generation

```

# Excute the evolution of the first generation
def gene1stevolution(init_population):
    generation = []
    for array in init_population:
        generation.append(Surface(array))

    result_list = []
    for individual in generation:
        result = getdeltaDisp(individual)
        dellckfile()
        result_list.append(result)

    writetolog(result_list)

    sorted_result_list = result_list[:]
    sorted_result_list.sort()
    templist = sorted_result_list[:selected_no]
    selected = []
    for i in templist:
        selected.append(init_population[result_list.index(i)])
    evolved_population = []

```

```

for i in range(int(population_size/2)):
    male = random.randrange(len(selected))
    female = random.randrange(len(selected))
    if female == male:
        female = random.randrange(len(selected))
    else:
        pass
    parent_male = selected[male][:]
    parent_female = selected[female][:]
    chromosome_crossover(parent_male,parent_female)
    adjusting(parent_male)
    adjusting(parent_female)
    mutate(parent_male)
    mutate(parent_female)
    evolved_population.append(parent_male)
    evolved_population.append(parent_female)
return evolved_population

```

```

# Excute the evolution of the generations from the second
def evolution(evolved_population):
    global init_population
    init_population = evolved_population
    return gene1stevolution(init_population)

```